High-precision optical polarimetry as a tool to learn about orbital orientation and nature of optical emission of black hole X-ray binaries

Juri Poutanen (Univ. of Turku, Finland; IKI, Moscow)
with
A. Veledina, A. Berdyugin, J. Kajava, I. Kosenkov, V. Kravtsov, V. Piirola,
S. Tsygankov (Univ. of Turku), S. Berdyugina (KIS),
T. Sakanoi, M. Kagitani (Tohoku), M.A.P. Torres (IAC),
P. Jonker (SRON), H. Jermak, M. Shrestha (Liverpool)

April 29, 2022

Plan

1. Motivation
2. Previous significant OIR polarimetric observations of black hole X-ray binaries
3. New instruments: high-precision polarimeters DIPol-2 and DIPol-UF
4. DIPol-2 results on V404 Cyg
5. DIPol-2 results on MAXI J1820+070
6. DIPol-UF results on MAXI J1820+070
7. Future: X-ray polarimetry
8. Conclusions

1. Motivation

Black holes in X-ray binaries

- Bright X-ray sources powered by a release of gravitational energy of gas accreted from a companion.

- Some of unsolved problems (for todays talk):

1. Nature of optical emission
2. Inclination of the black hole spin to the orbital spin

- Polarization may provide a clue to these questions.

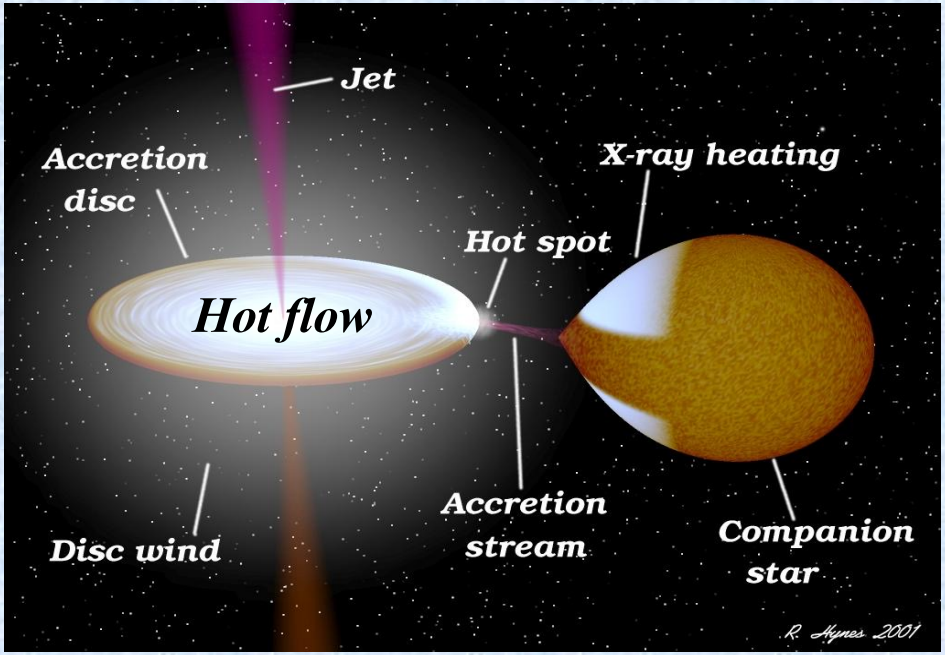

Broadband spectrum of GX 339-4

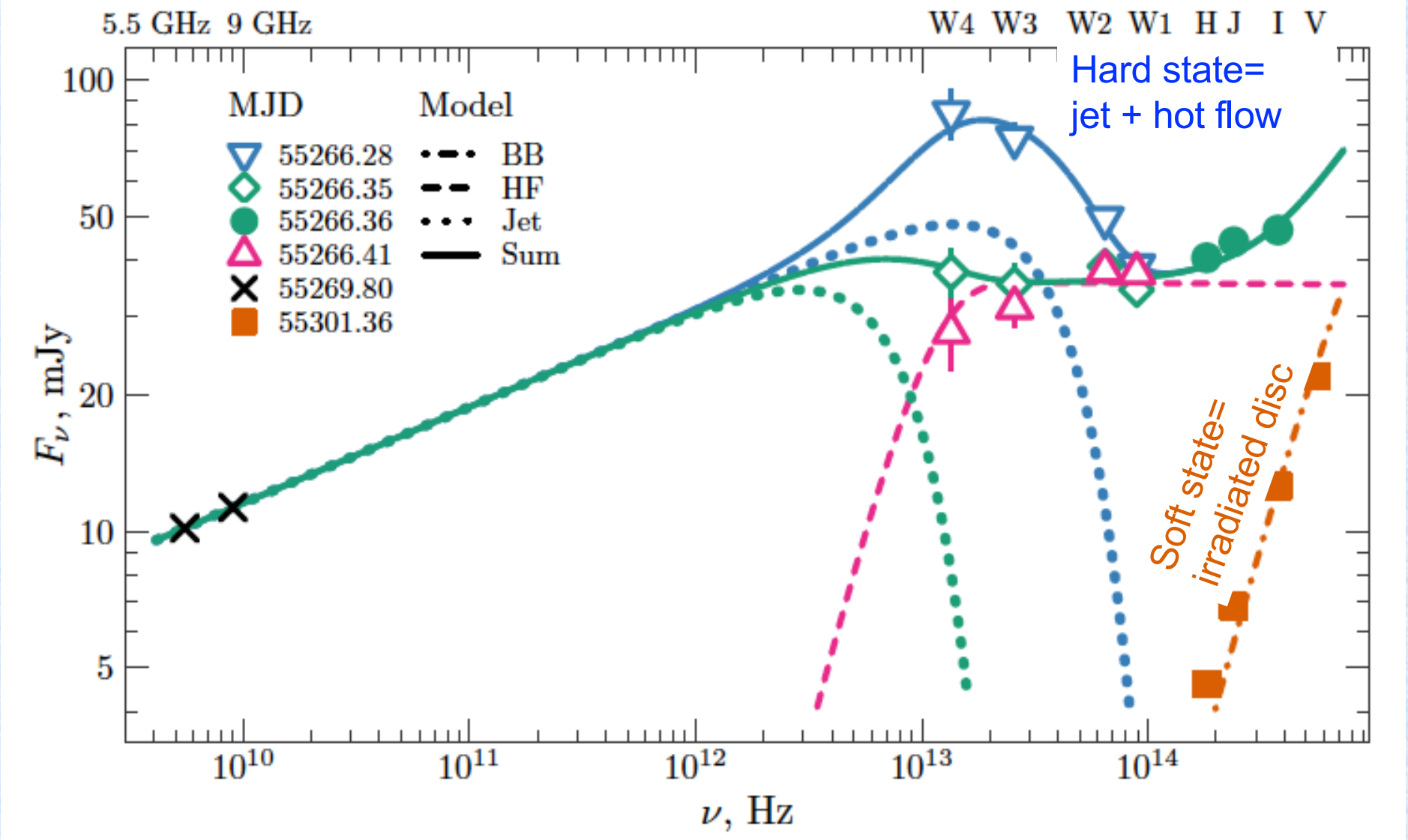

Kosenkov et al. 2020

Black holes in X-ray binaries

- Polarization may provide information about the source of emission, geometry of the emitting zone, inclination.
- Polarization also gives information about orientation.

In black hole X-ray binaries polarization may arise from
(1) Synchrotron radiation in the jet or hot flow

(2) Scattering (by electrons or dust) of the disc radiation in the (optically thin) hot flow/wind/jet

(3) Scattering within the (optically thick) disc or the envelope

(4) Interstellar polarization due to dichroism of ISM dust

2. Previous results

Polarization of black hole X-ray binaries

Kemp et al. (1978)

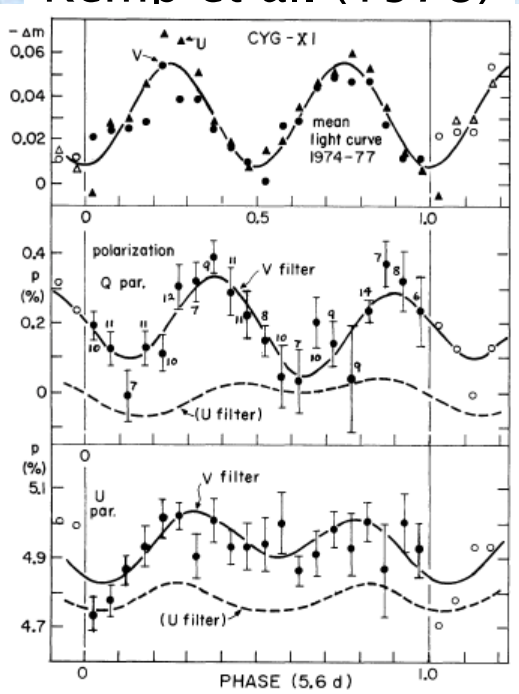

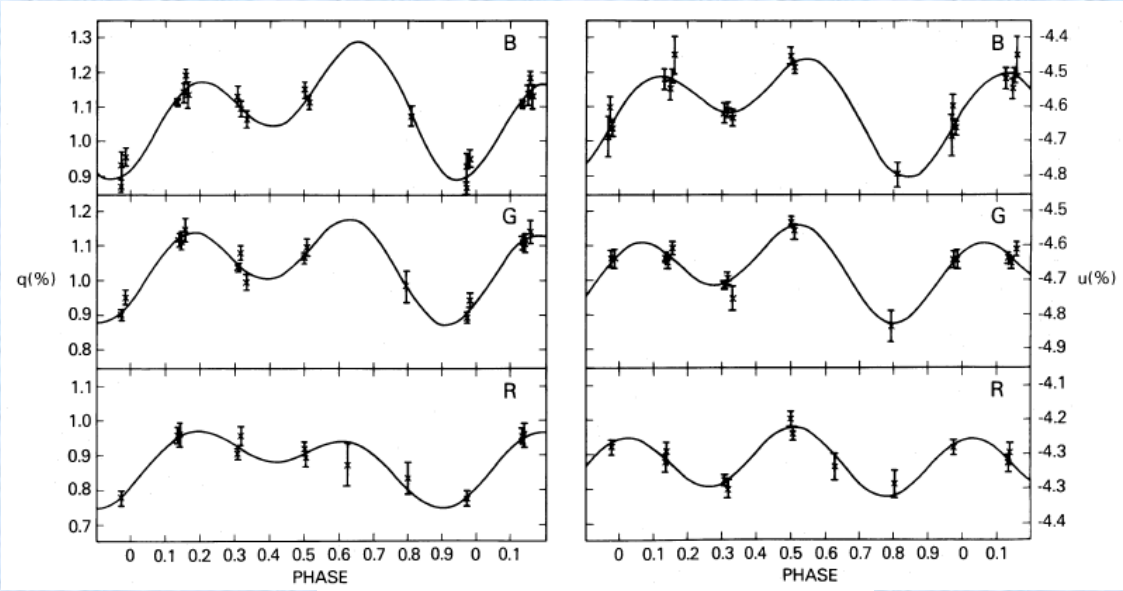

Dolan & Tapia (1989)

Detection of phase-dependent polarization in Cyg X-1 by Kemp et al. (1978) [i=76 deg], Dolan & Tapia (1989) [i=118 (62+5-37) deg] and Nagae et al. (2009) [i=30+-16) deg].

Origin in scattering by a focused wind?

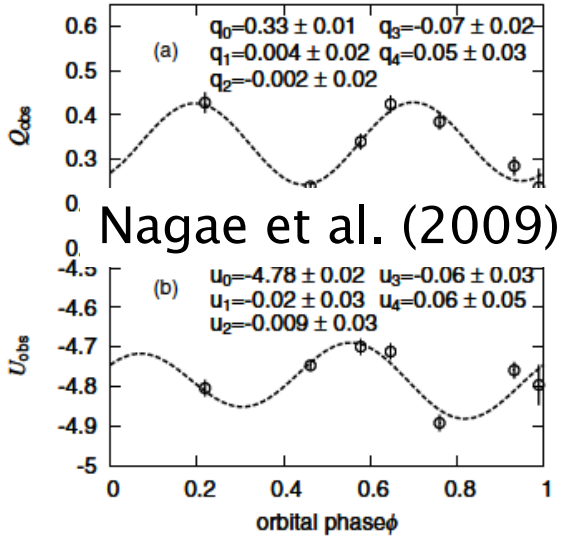

Nagae et al. (2009)

2. Previous results

Polarization of black hole X-ray binaries

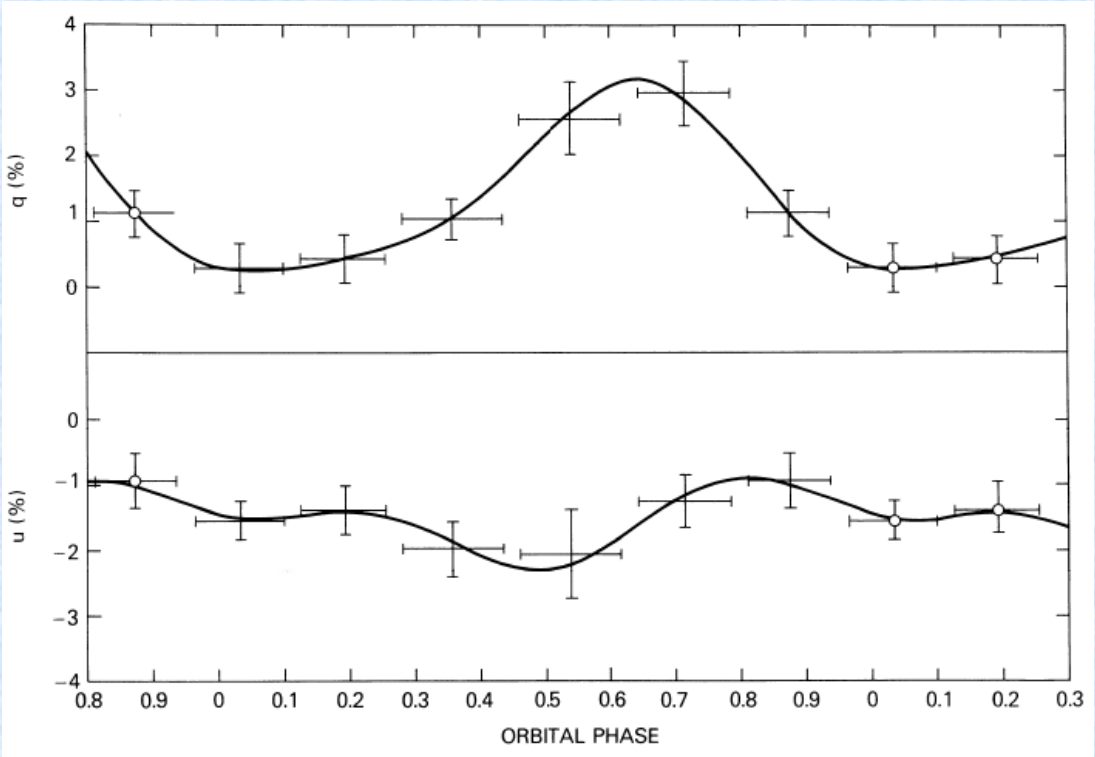

Detection of phase-dependent ~3% polarization in A 0620-00 in quiescence by Dolan & Tapia (1989) with 4.5 m MMT.

In the outburst the polarization (1.7%, PA=140 deg) is close to the ISM values (Dolan & Tapia 1976).

2. Previous results Polarization of black hole X-ray binaries

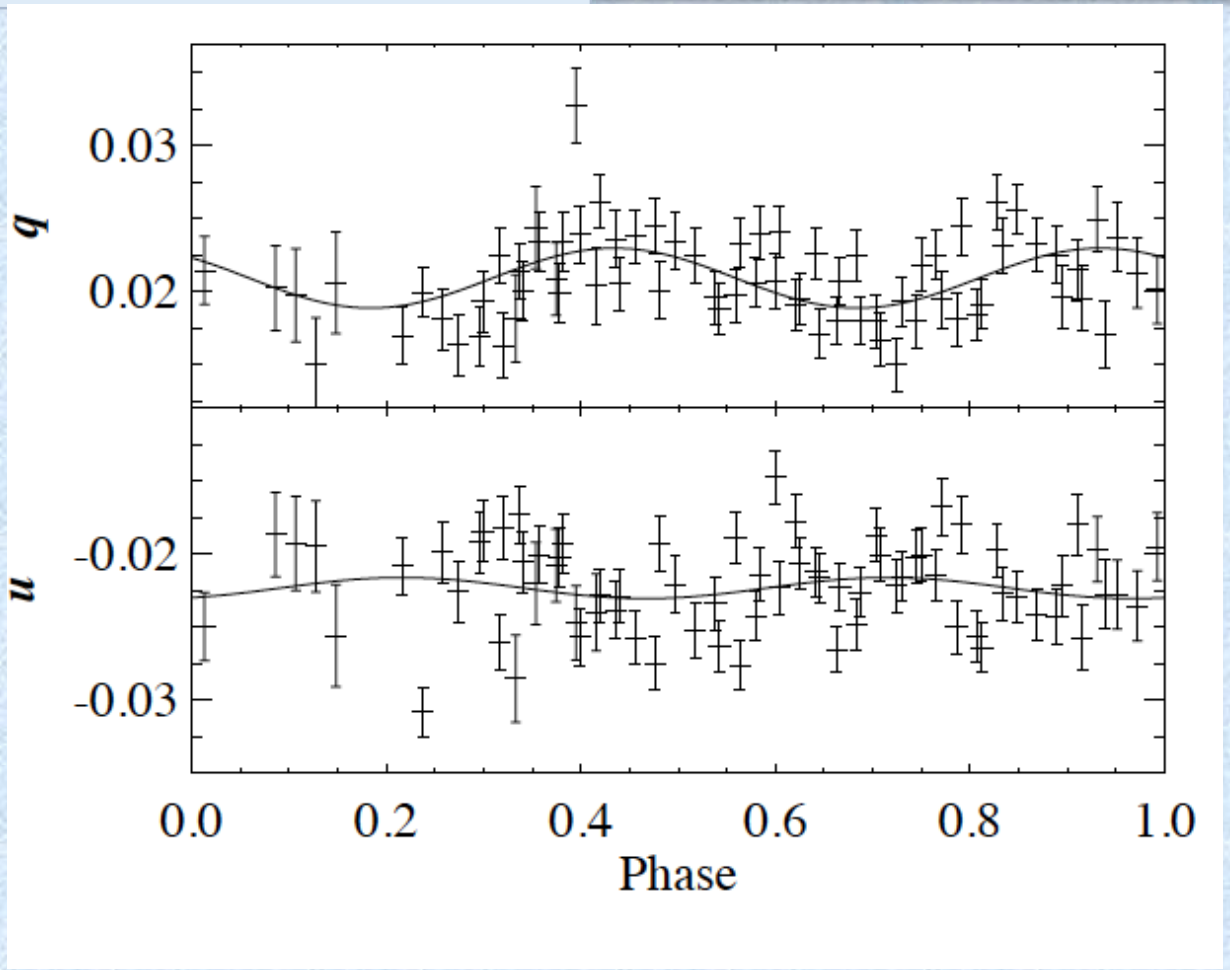

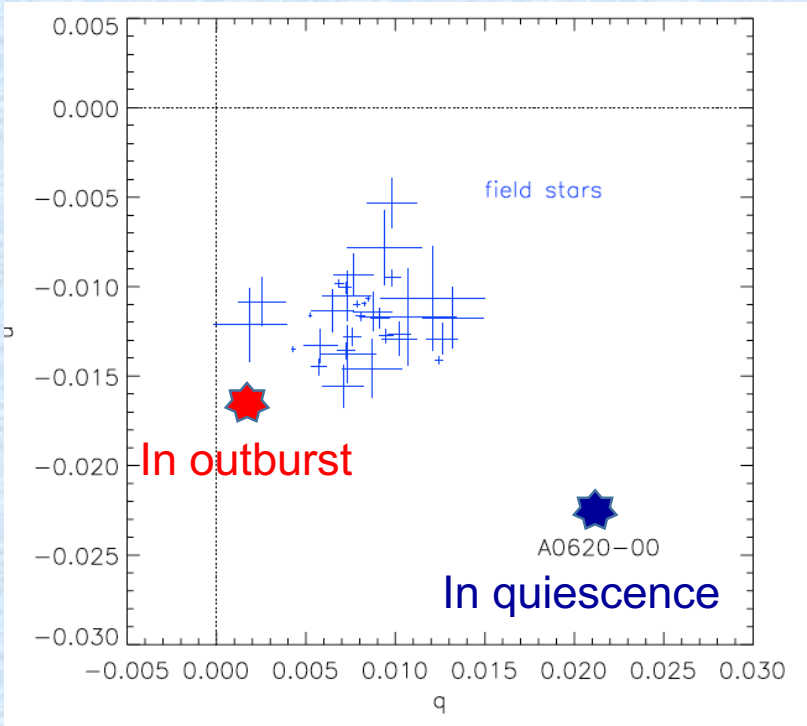

.. and non-detection of phase-dependent polarization in A 0620-00 in quiescence by Dubus et al. (2008) with ESO 3.6 m using EFOSC2.

Intrinsic polarization of about 2%.

Polarization of black hole X-ray binaries

Russell & Fender (2008) claim detection of intrinsic linear polarization in NIR in GRO J1655-40 (4-7%)

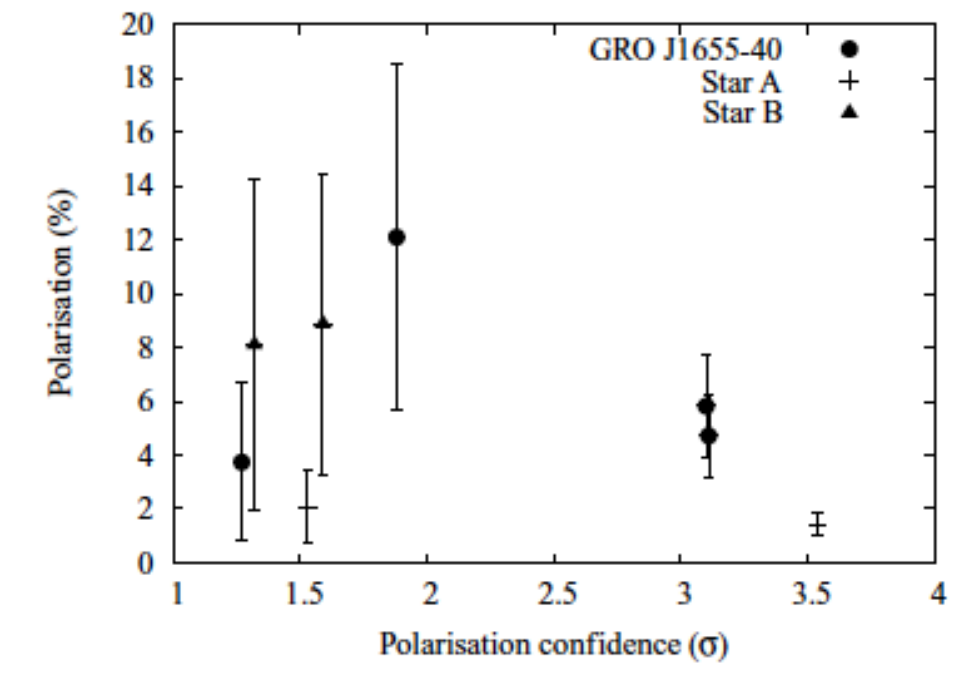

They applied Serkowski's law $p_V < 3A_V$ to K-band assuming $p_K = (A_K/A_V)\, p_V = 0.1 p_V$ while typically observed (Whittet+'92) $p_K = (0.2\text{-}0.6) p_V$

The ISM polarization was underestimated.

GX 339-4 – ISM polarization
A number of non-constraining upper limits (<16%).

Polarization of black hole X-ray binaries

Russell+'16: Swift J1357.2− 0933 LP=8.0±2.5%.

		P	PA	σ
1	J	6.84 ± 4.17	18.2 ± 14.9	1.64
2	J	$3.16^{+3.60}_{-3.16}$	38.0 ± 21.5	0.88
2	K_S^b	6.41 ± 5.65	159.0 ± 18.9	1.13
1+2	J	7.27 ± 2.74	25.4 ± 10.1	2.65
1+2	K_S^b	8.44 ± 4.76	0.4 ± 14.1	1.77
1+2	$J + K_S$	8.00 ± 2.48	14.6 ± 8.5	3.22
	– Field star[c] close to Swift J1357.2−0933 –			
1+2	$J + K_S$	$0.54^{+1.12}_{-0.54}$	75.2 ± 32.7	0.48

The results are marginally significant.
ISM polarization is difficult to determine from one field star – one needs to know the distance to the source and field star.

Polarization of black hole X-ray binaries

- It is important to measure ISM contribution to the observed polarization.
- It is important to properly calibrate the data by observing zero polarization and high-polarization standards.

3. New instruments

Double Image Polarimeter: DIPol-2

- Two orthogonally polarized images are recorded simultaneously: no errors due to variations in transparency and seeing
- Two orthogonally polarized sky images overlap: sky polarization is eliminated automatically
- Single measuring cycle consists of 16 rotations: rotationally induced small internal errors, arising from dust particles on retarder, are eliminated
- Standard calibration procedure: bias and dark subtraction + flat fielding

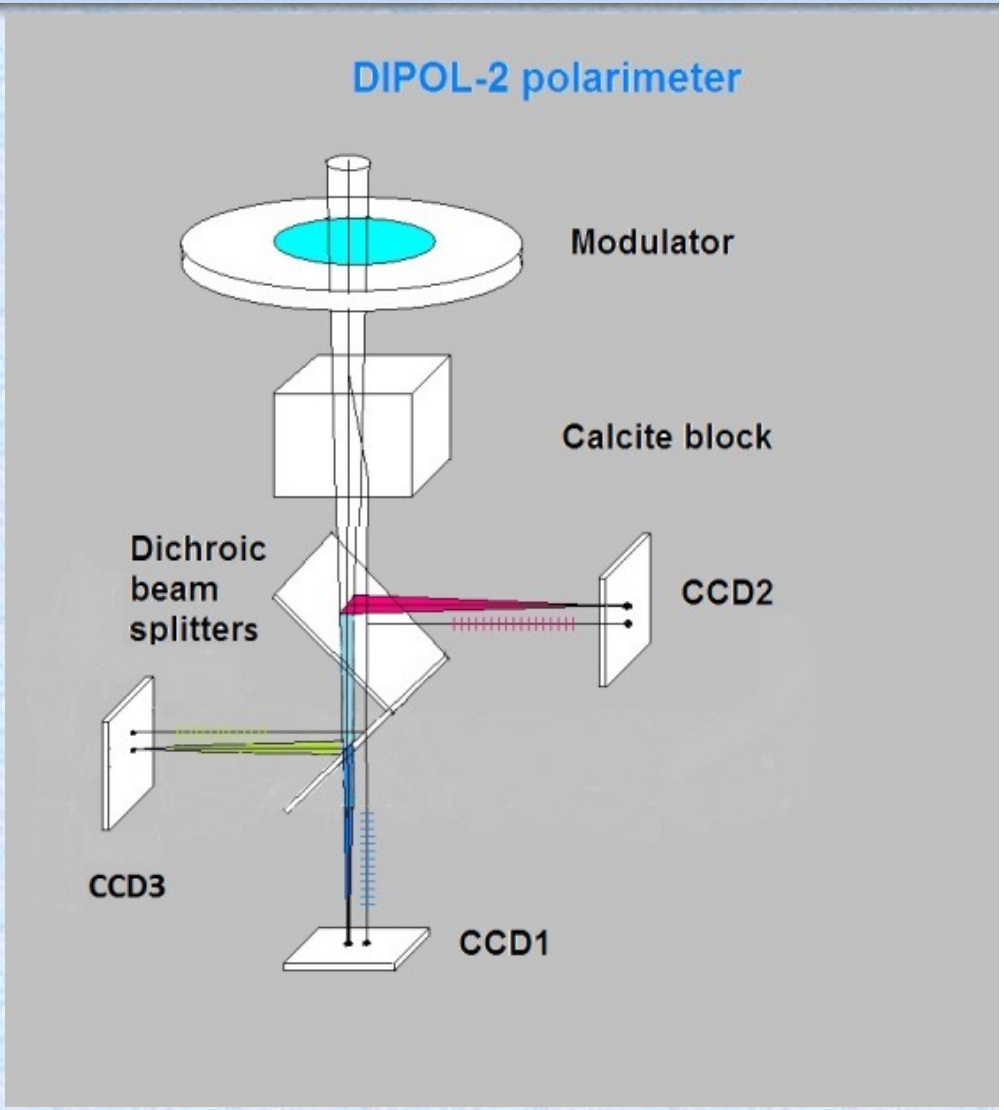

- Instrumental polarization $<10^{-4}$, can be determined to accuracy of 10^{-6}
- Typically achieved accuracy for bright sources $<10^{-5}$.

Piirola et al. 2014

3. New instruments

DIPol-2: High-Precision Three-Band CCD Polarimeter

KVA – La Palma

UH88 – Mauna Kea

WHT – La Palma

T60 - Haleakala

H127 – Bisdee Tier

3. New instruments

DIPol-Ultra Fast

- Polarization unit: discretely rotated super-achromatic HWP + plane-parallel calcite
- Two dichroic mirrors for the wavelength separation (simultaneous measurements in the B_J, V_J, R_c passbands)
- Retractable polarization unit
- Two high-grade stepper motors: for HWP rotation and polarization unit retraction
- Normal and fast photometry modes
- Three ANDOR iXon Ultra 897 cameras
- Each CCD camera is controlled with separate industrial-grade mini-PCs linked together into high-speed local network
- Optimized for usage with the large-aperture telescopes
- Designed to be used remotely

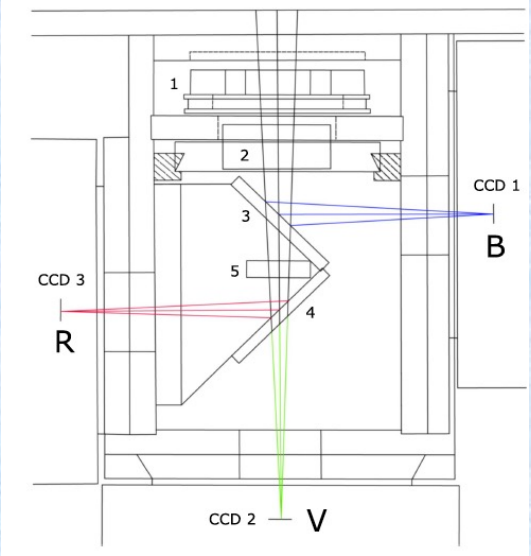

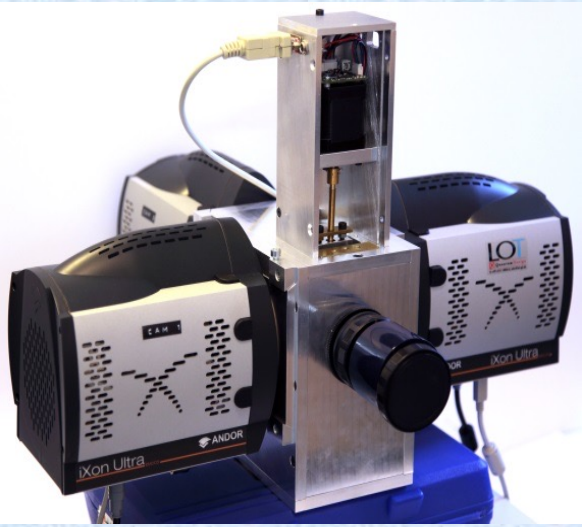

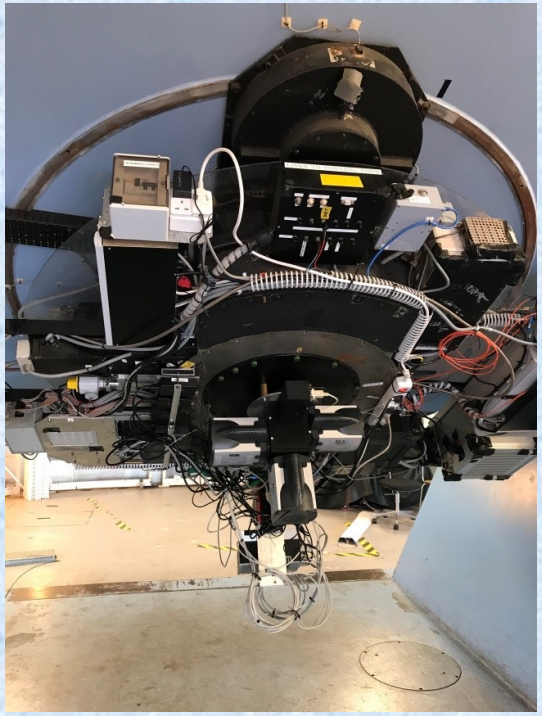

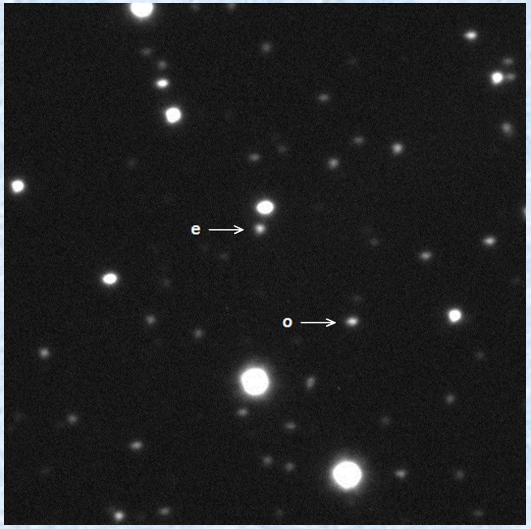

Piirola et al. 2021

V404 Cyg

- Optical nova of 1938
- X-ray outburst in 1989 discovered by Ginga: GS2023+33
- Orbital period 6.5 days (Casares et al. 1992)
- Distance = 2.39 ± 0.14 kpc (Miller et al. 2009)
- Mass function $6.26 \pm 0.31\ M_{\odot}$

4. DIPol-2

2015 outburst of V404 Cyg

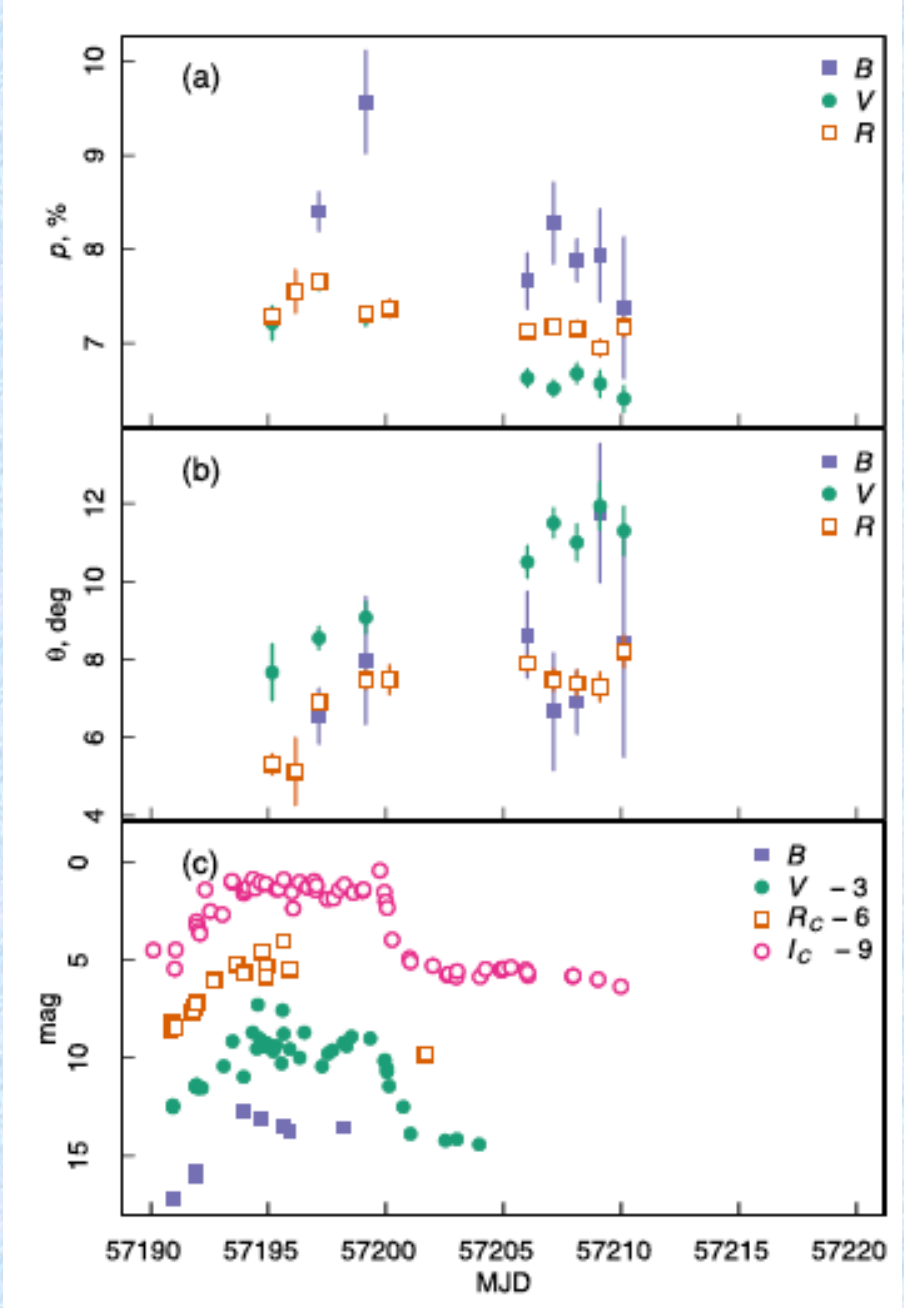

Polarization data during outburst with DIPol-2 at the 60 cm KVA

In quiescence: DIPol-2 at 4.2m WHT.

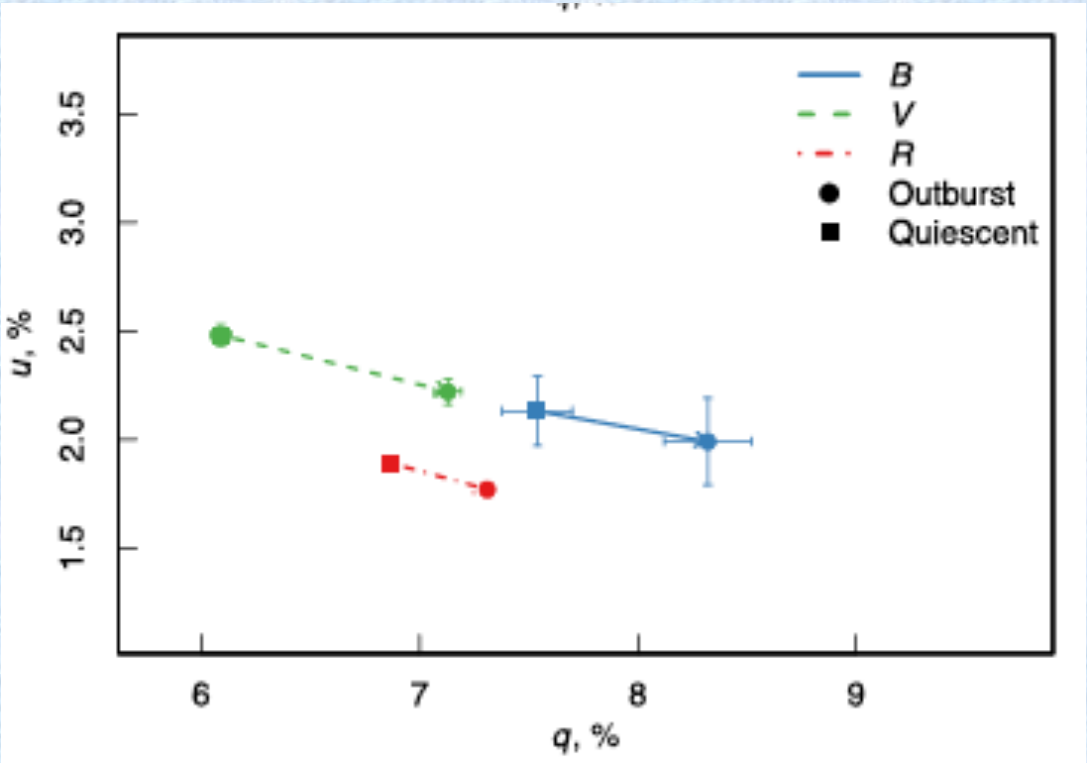

Kosenkov et al. (2017)

2015 outburst of V404 Cyg

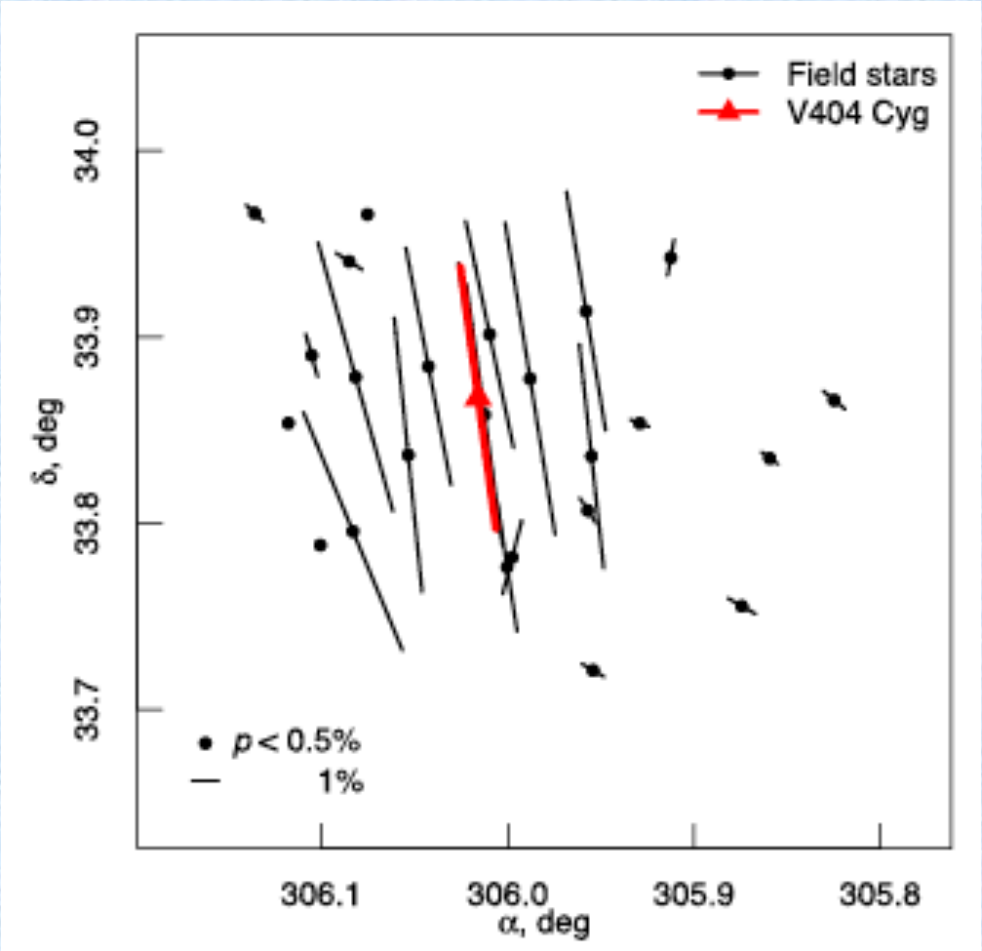

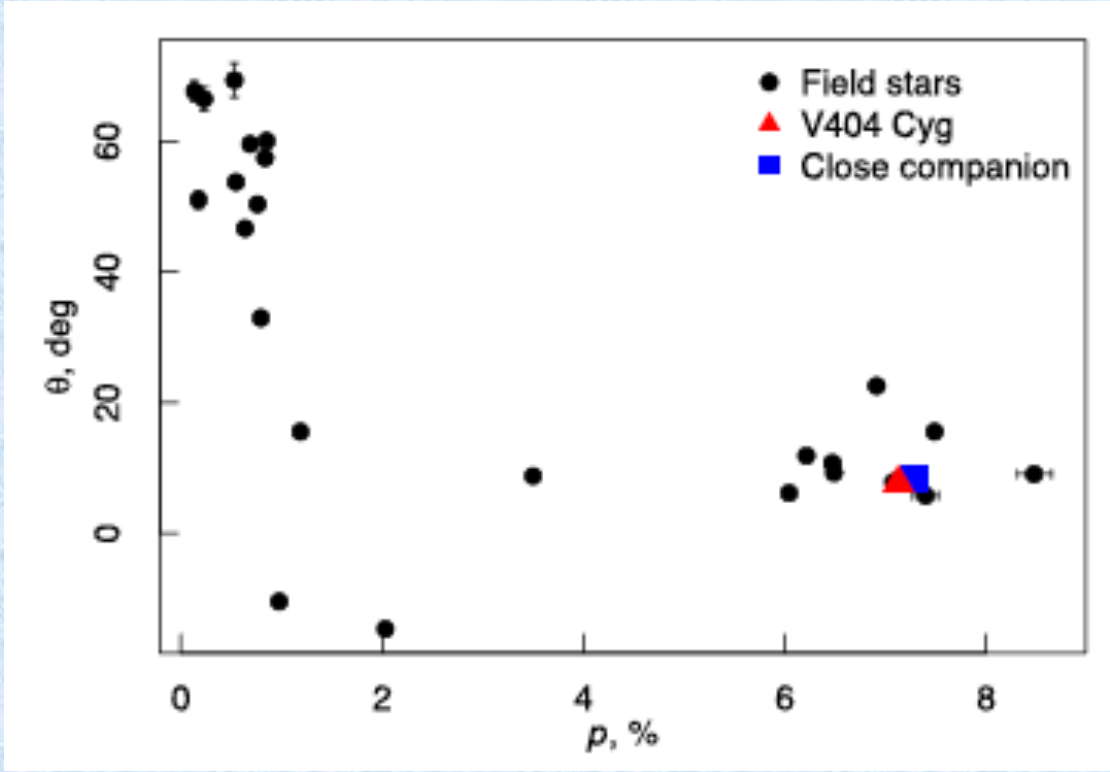

Polarization of V404 Cyg in quiescence is consistent with the nearby field stars (including a close companion) implying ISM origin.

Kosenkov et al. (2017)

2015 outburst of V404 Cyg

The intrinsic polarization is smaller in R-band ➔
not the jet

PA varies between -30 and 0 deg.

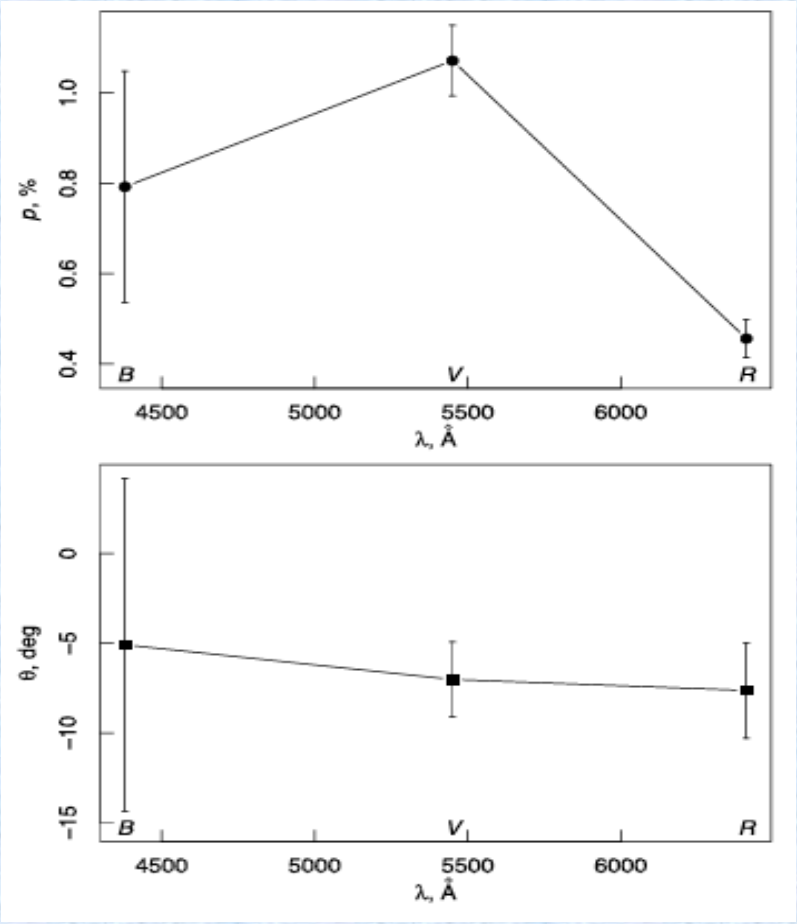

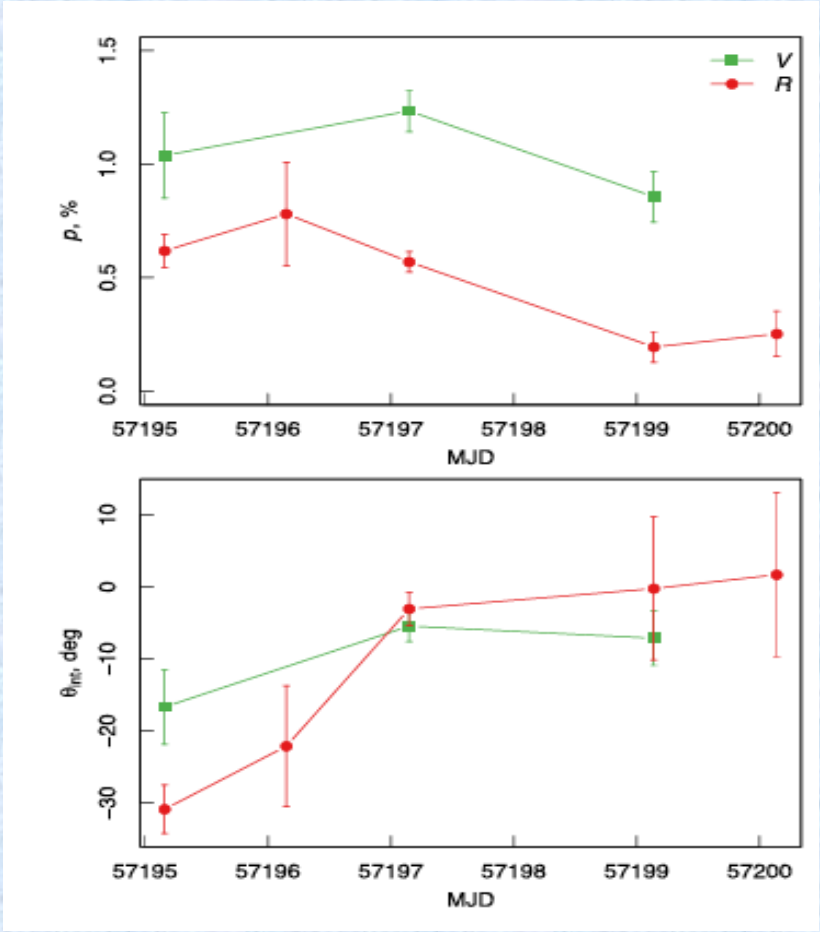

Kosenkov et al. (2017)

4. DIPol-2

2015 outburst of V404 Cyg

The intrinsic polarization is smaller in R-band ➔ not the jet

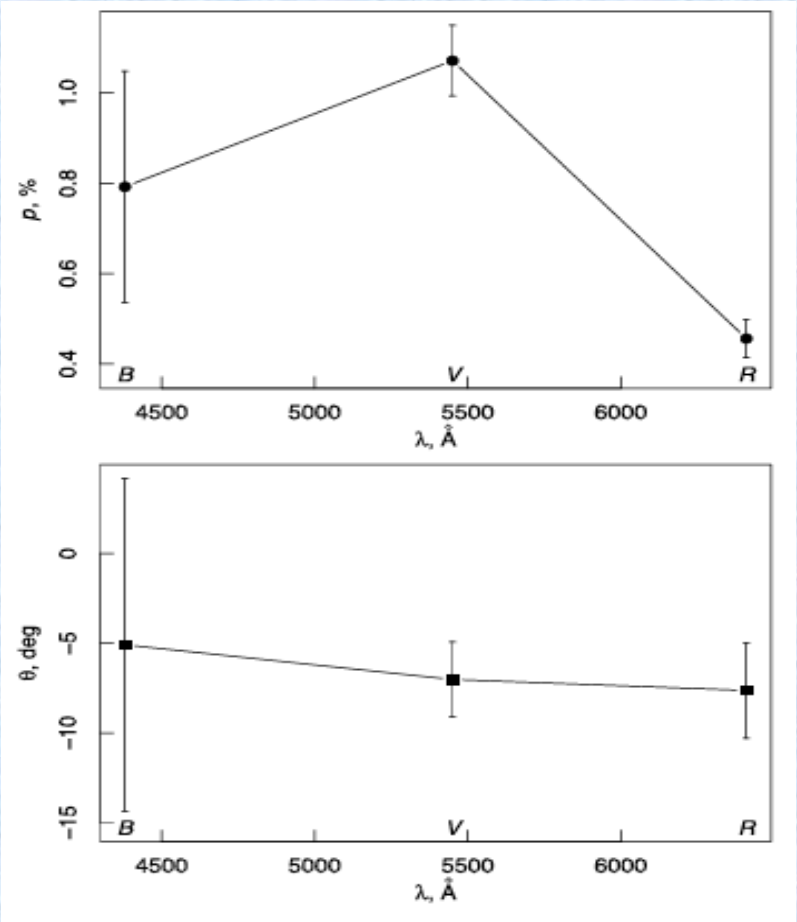

Kosenkov et al. (2017)

However, PA are consistent with position angle of ejections observed with VLBI (Miller-Jones et al. 2019)

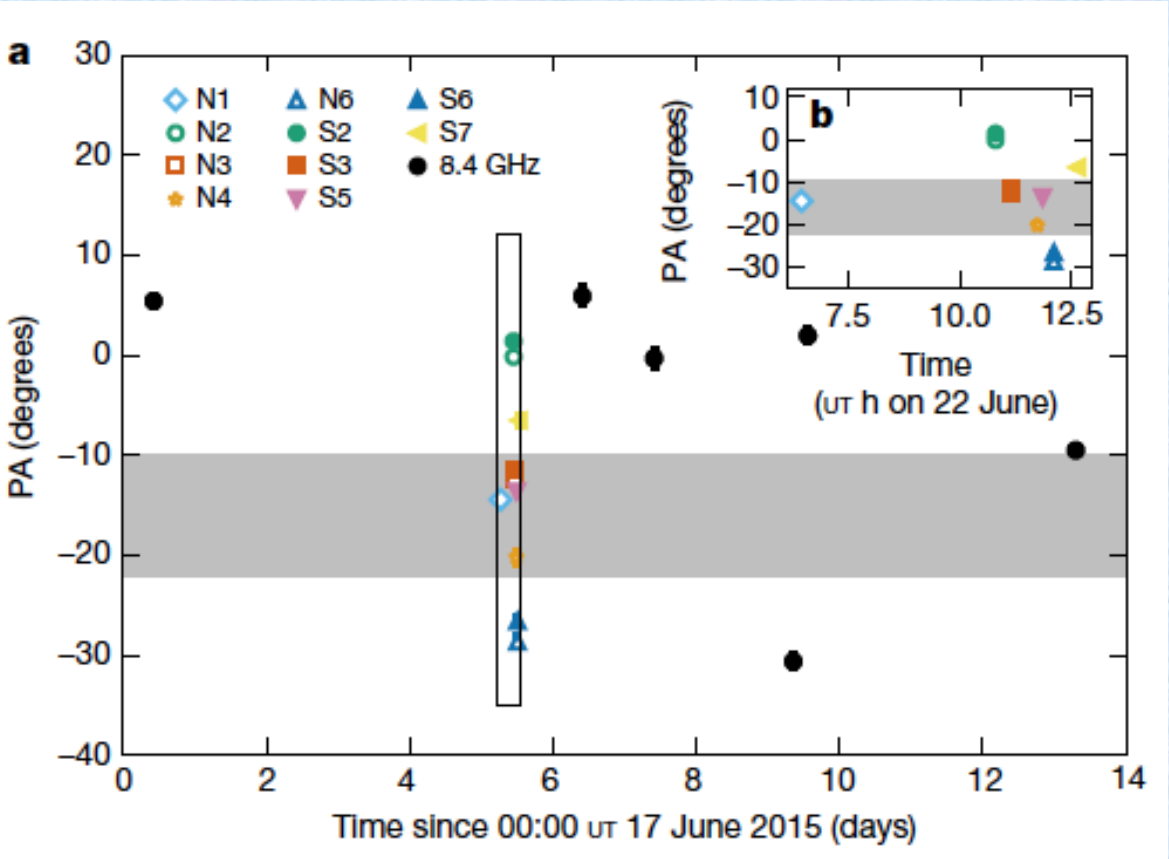

2015 outburst of V404 Cyg

The intrinsic polarization is smaller in R-band ➔ not the jet

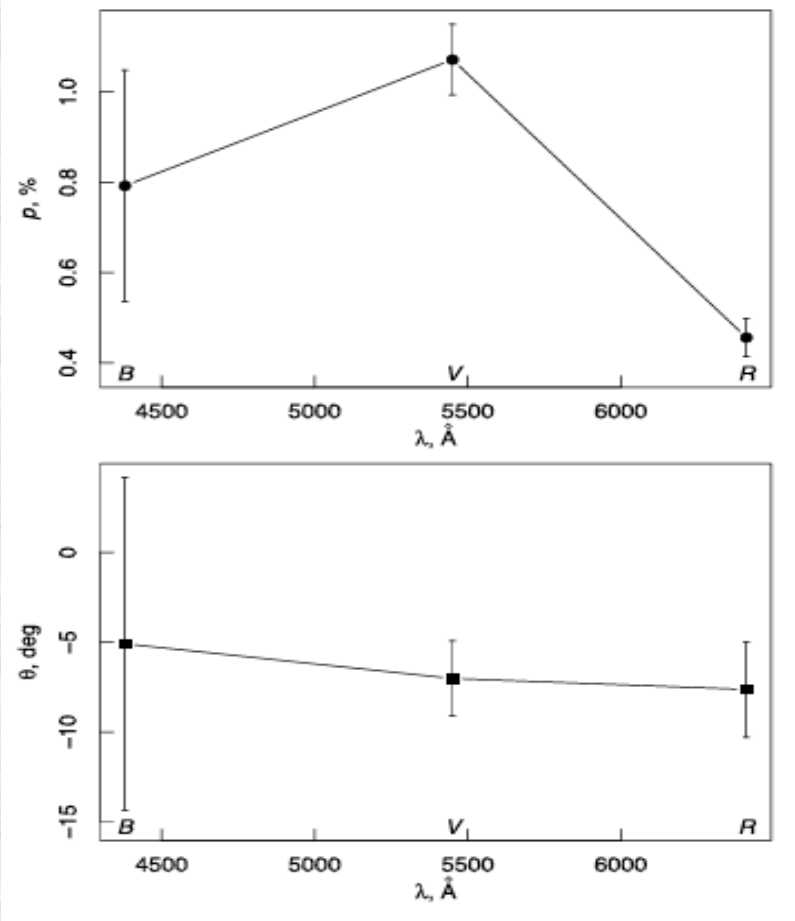

Kosenkov et al. (2017)

But where it comes from? Likely non-spherical outflow / equatorial wind. Wavelength dependence resembles that of Be stars (Poeckert et al. 1979). Results from interplay between scattering and absorption (Nagirner [1962] effect).

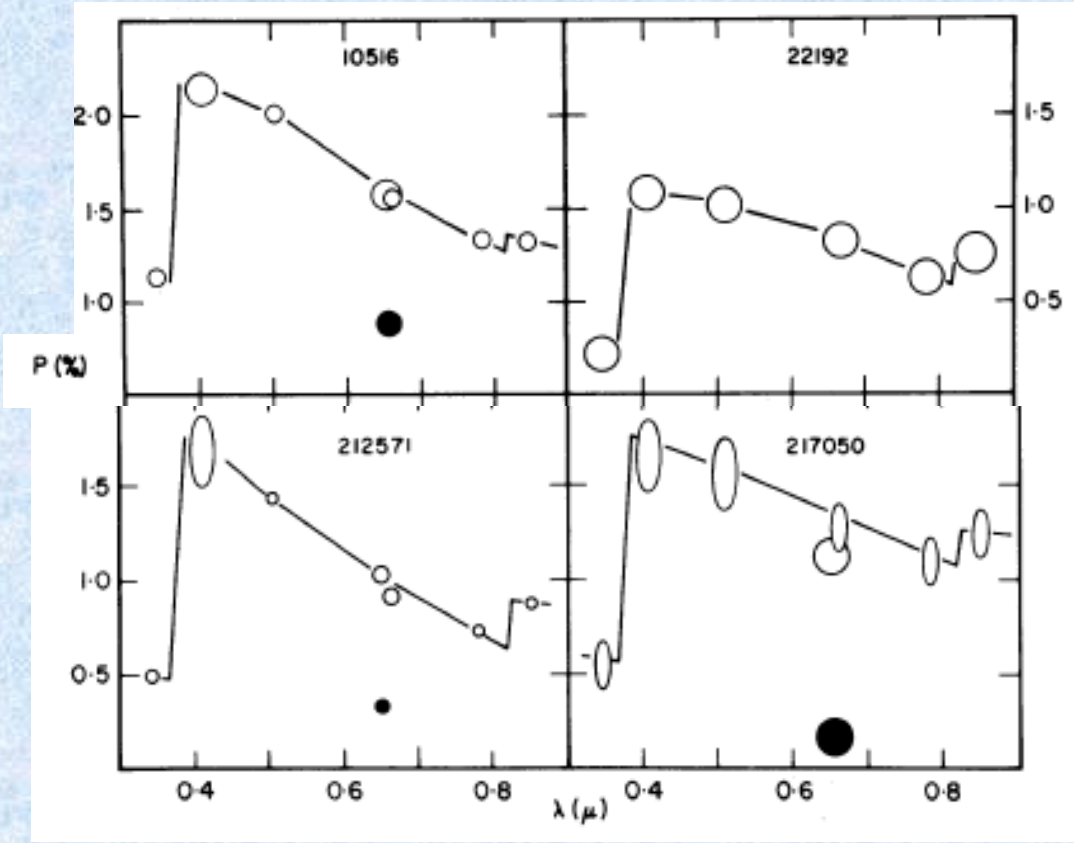

5. DIPol-2

MAXI J1820+070

- First detected in March 2018 by MAXI X-ray monitor (Kawamuro et al. 2018)
- Identified with optical transient ASASSN-18ey (Denisenko 2018, Tucker et al. 2018)
- Orbital period 0.685 days (Torres et al. 2019)
- Mass function $5.18 \pm 0.15\ M_{\odot}$ (Torres et al. 2019)
- Orbit inclination $66 < i_{orb} < 81$ deg (Torres et al. 2020)
- Distance = 2.96 ± 0.33 kpc (Atri et al. 2020)
- Jet inclination $i_{jet} = 63 \pm 3$ deg (Atri et al. 2020)
- Radio jet PA = 25.8 ± 4.4 deg (Kosenkov et al. 2020; Bright et al. 2020)
- X-ray jet PA = 25.1 ± 1.4 deg (Espinaisse et al. 2020)

MAXI J1820+070 in outburst

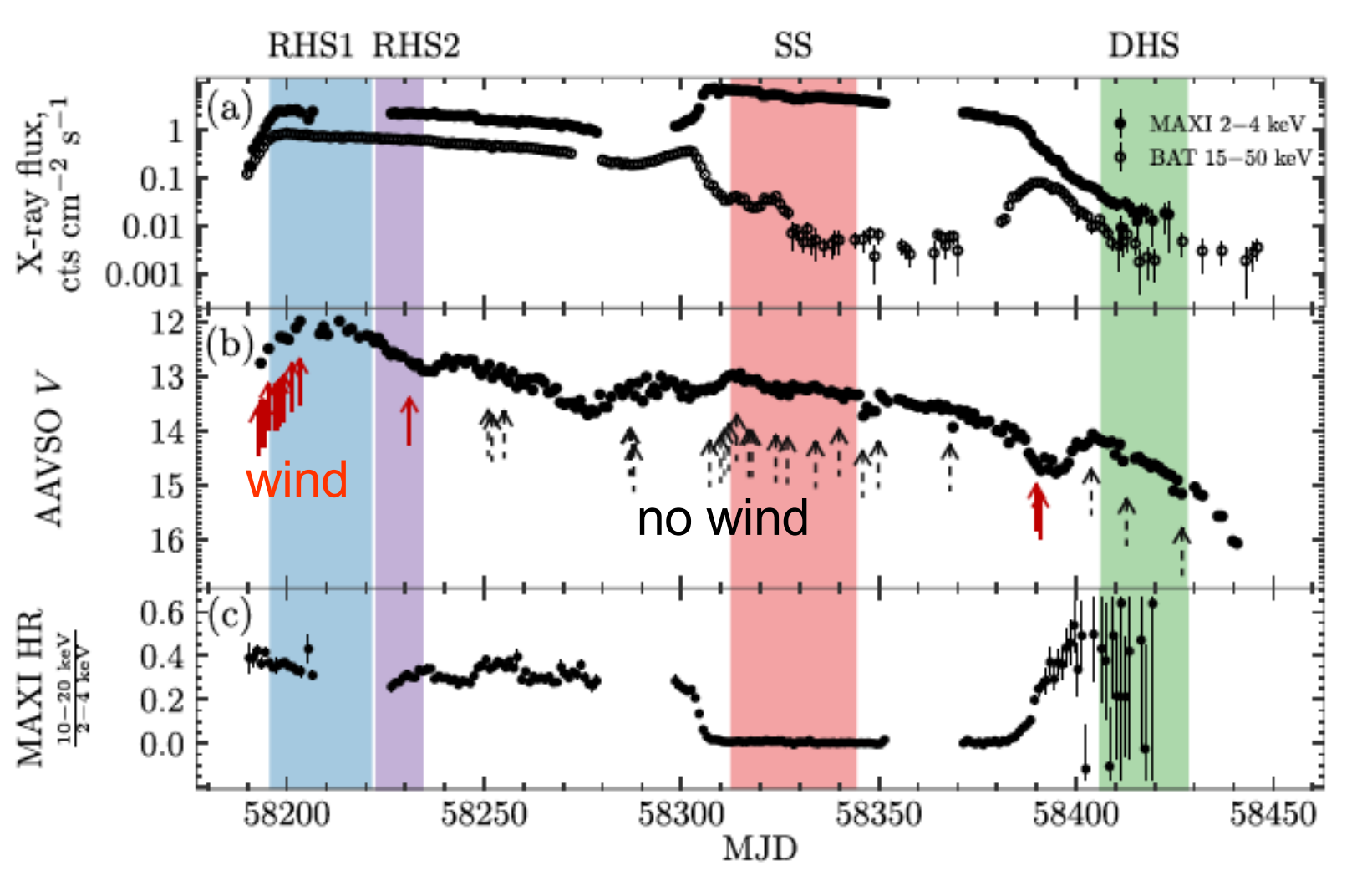

Veledina et al. (2019), Kosenkov et al. (2020)

5. DIPol-2

MAXI J1820+070 : ISM polarization

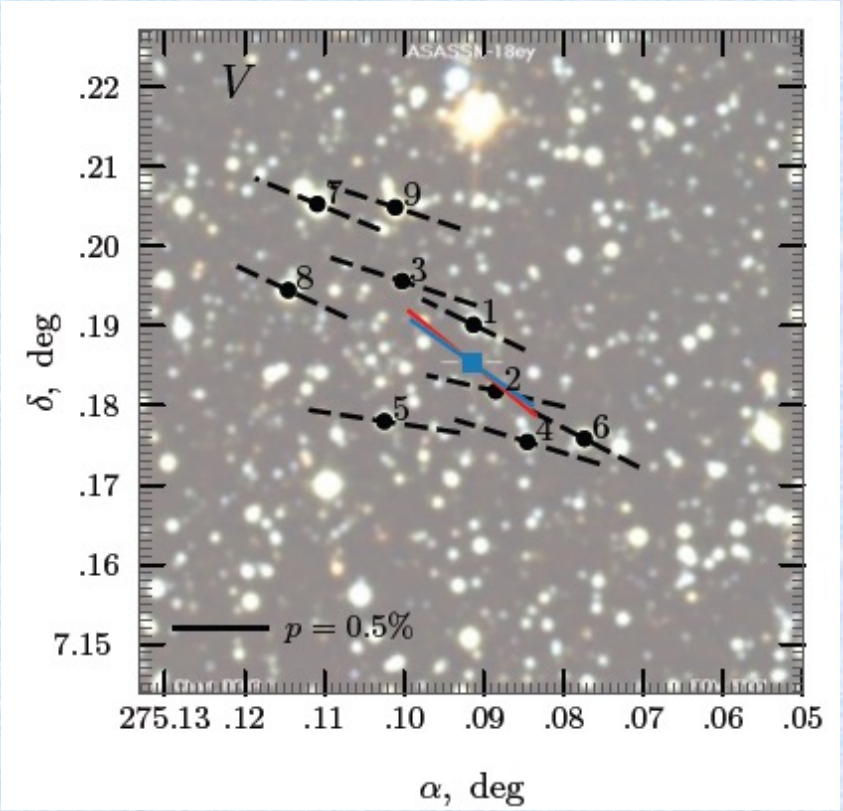

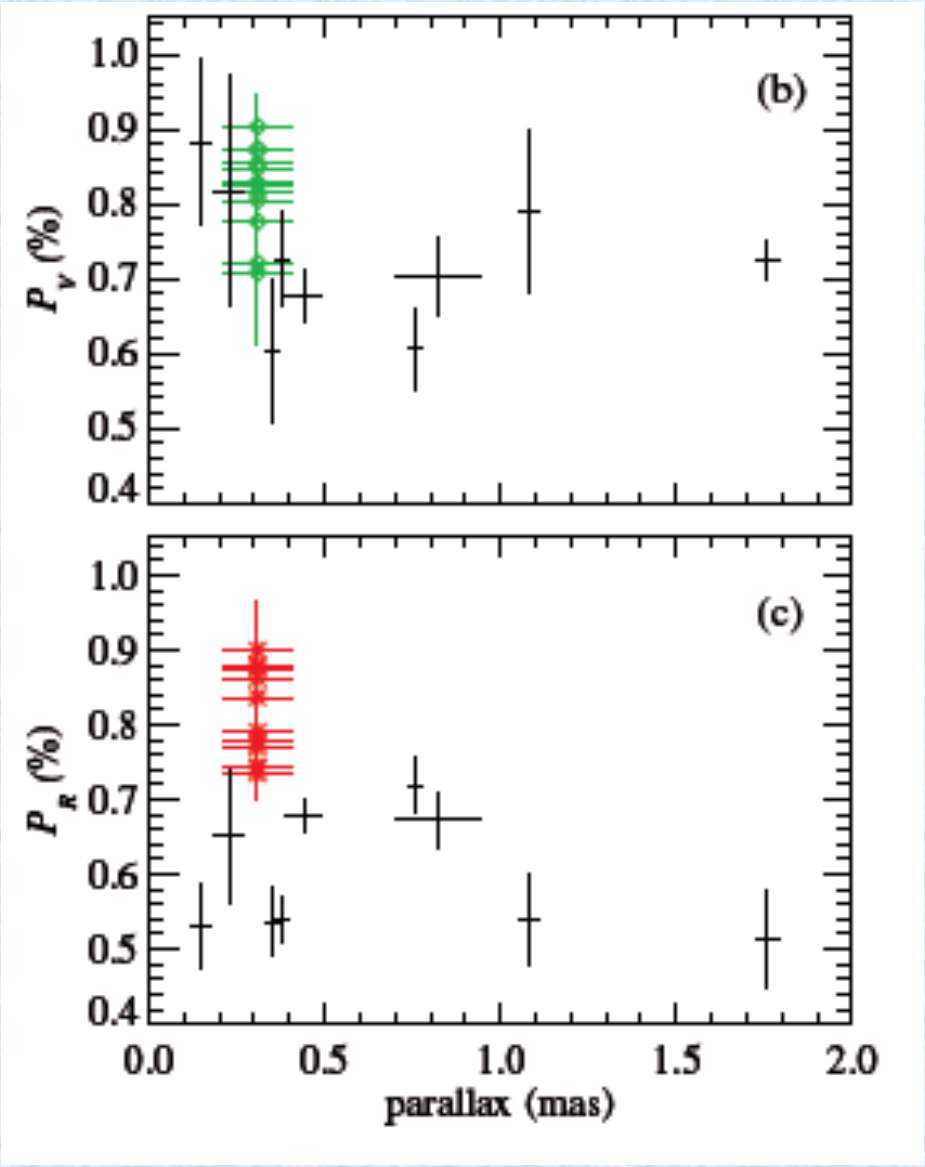

Polarization of the source (red and blue “vectors”) is different from that of the field stars (black vectors).

Veledina et al. (2019)

MAXI J1820+070 : ISM polarization

Table 2. Polarimetric data for the field stars and their weighted average.

		B		*V*		*R*	
Star	π (mas)	P (%)	PA (°)	P (%)	PA (°)	P (%)	PA (°)
1	0.76 ± 0.02	0.80 ± 0.06	60.4 ± 2.1	0.60 ± 0.06	63.7 ± 2.7	0.69 ± 0.05	65.1 ± 1.9
2	0.23 ± 0.04	0.75 ± 0.24	82.3 ± 8.7	0.74 ± 0.17	77.1 ± 6.6	0.65 ± 0.10	69.9 ± 4.5
3	0.15 ± 0.03	0.81 ± 0.16	67.3 ± 5.5	0.82 ± 0.13	71.9 ± 4.4	0.52 ± 0.07	74.9 ± 3.6
4	1.76 ± 0.03	0.49 ± 0.11	70.7 ± 6.6	0.79 ± 0.13	73.0 ± 4.9	0.51 ± 0.07	75.5 ± 4.1
5	1.08 ± 0.03	0.81 ± 0.09	68.6 ± 3.2	0.80 ± 0.12	81.4 ± 4.1	0.61 ± 0.07	75.0 ± 3.2
6	0.35 ± 0.02	0.80 ± 0.08	59.8 ± 3.0	0.64 ± 0.11	62.3 ± 4.9	0.50 ± 0.05	62.9 ± 3.0
7	0.44 ± 0.05	0.82 ± 0.04	64.9 ± 1.4	0.70 ± 0.04	67.6 ± 1.6	0.67 ± 0.03	64.1 ± 1.1
8	0.82 ± 0.12	0.72 ± 0.07	65.6 ± 2.7	0.67 ± 0.07	64.9 ± 2.8	0.68 ± 0.04	66.2 ± 1.7
9	0.38 ± 0.02	0.74 ± 0.09	62.1 ± 3.3	0.71 ± 0.07	71.8 ± 2.8	0.53 ± 0.04	60.7 ± 1.9
2,3,6,7,9		0.80 ± 0.03	64.2 ± 1.2	0.70 ± 0.03	68.6 ± 1.3	0.60 ± 0.02	64.1 ± 0.9

Veledina et al. (2019)

MAXI J1820+070 in outburst

Table 1. The average observed and intrinsic polarization towards MAXI J1820+070 and the estimate of the ISM polarization. Errors are 1σ.

State	B P (per cent)	B θ (deg)	V P (per cent)	V θ (deg)	R P (per cent)	R θ (deg)
			Observed polarization			
RHS1[a]	0.76 ± 0.01	53.9 ± 0.3	0.79 ± 0.01	54.7 ± 0.4	0.76 ± 0.01	53.3 ± 0.3
RHS2[a]	0.76 ± 0.02	51.4 ± 0.6	0.87 ± 0.02	50.5 ± 0.8	0.86 ± 0.02	45.8 ± 0.6
SS	0.66 ± 0.01	61.5 ± 0.4	0.67 ± 0.01	62.2 ± 0.5	0.62 ± 0.01	63.5 ± 0.4
DHS	0.76 ± 0.04	62.2 ± 1.4	0.63 ± 0.06	64.1 ± 2.6	0.67 ± 0.04	62.0 ± 1.7
ISM	0.81 ± 0.03	64.0 ± 1.1	0.71 ± 0.03	68.4 ± 1.2	0.60 ± 0.02	64.4 ± 0.8
<stars 2,3,6,7,9>			Intrinsic polarization			
RHS1	0.28 ± 0.01	9.2 ± 1.0	0.36 ± 0.01	22.9 ± 1.0	0.30 ± 0.01	29.0 ± 0.9
RHS2	0.34 ± 0.02	8.8 ± 1.4	0.51 ± 0.02	23.4 ± 1.4	0.53 ± 0.02	23.9 ± 1.1
SS	0.16 ± 0.01	−15.8 ± 1.6	0.15 ± 0.01	13.4 ± 2.3	0.02 ± 0.01	39.1 ± 11.0
DHS	0.06 ± 0.04	−3.0 ± 15.4	0.13 ± 0.06	2.8 ± 12.4	0.09 ± 0.04	44.8 ± 12.5

Veledina et al. (2019), Kosenkov et al. (2020)

MAXI J1820+070 in outburst

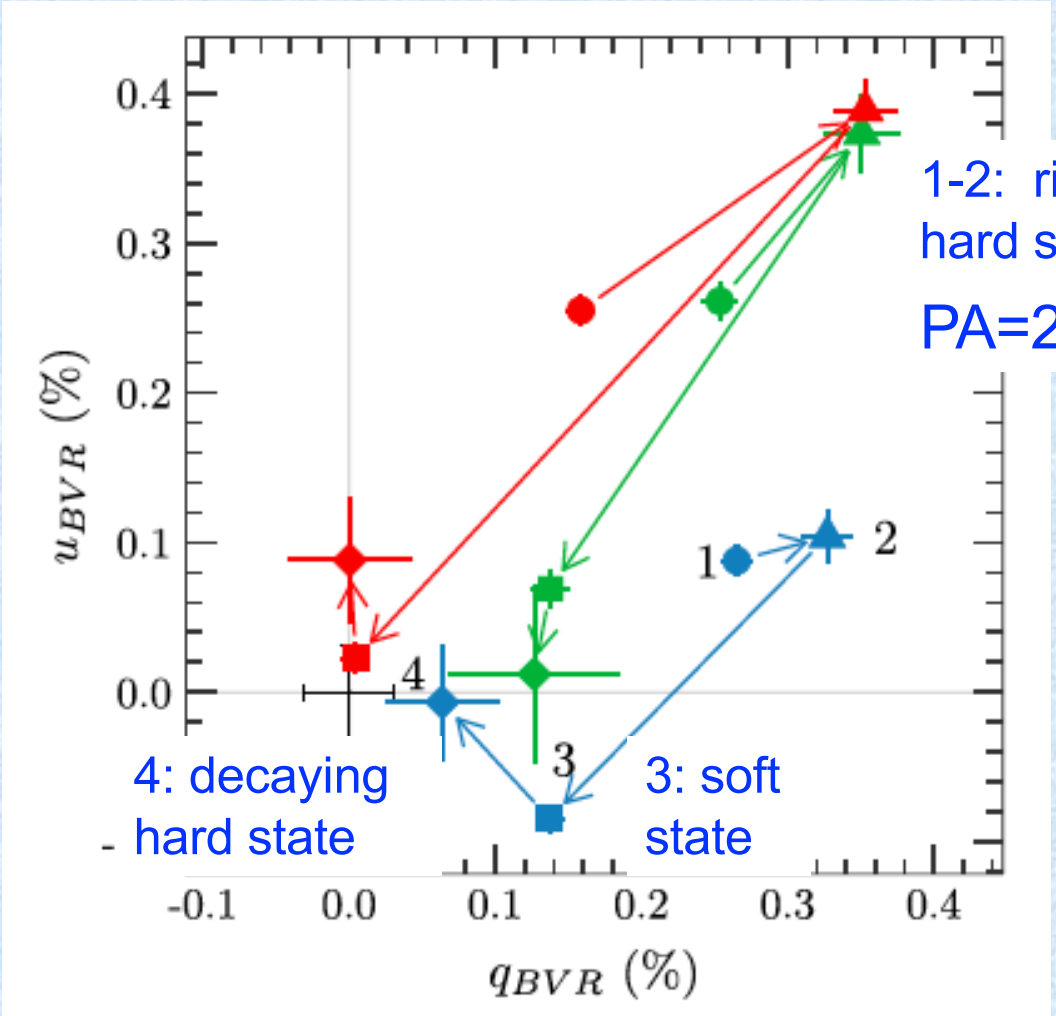

In B, there is likely an additional component with different PA.

Kosenkov et al. (2020)

Chandra

X-ray jets from MAXI J1820+070

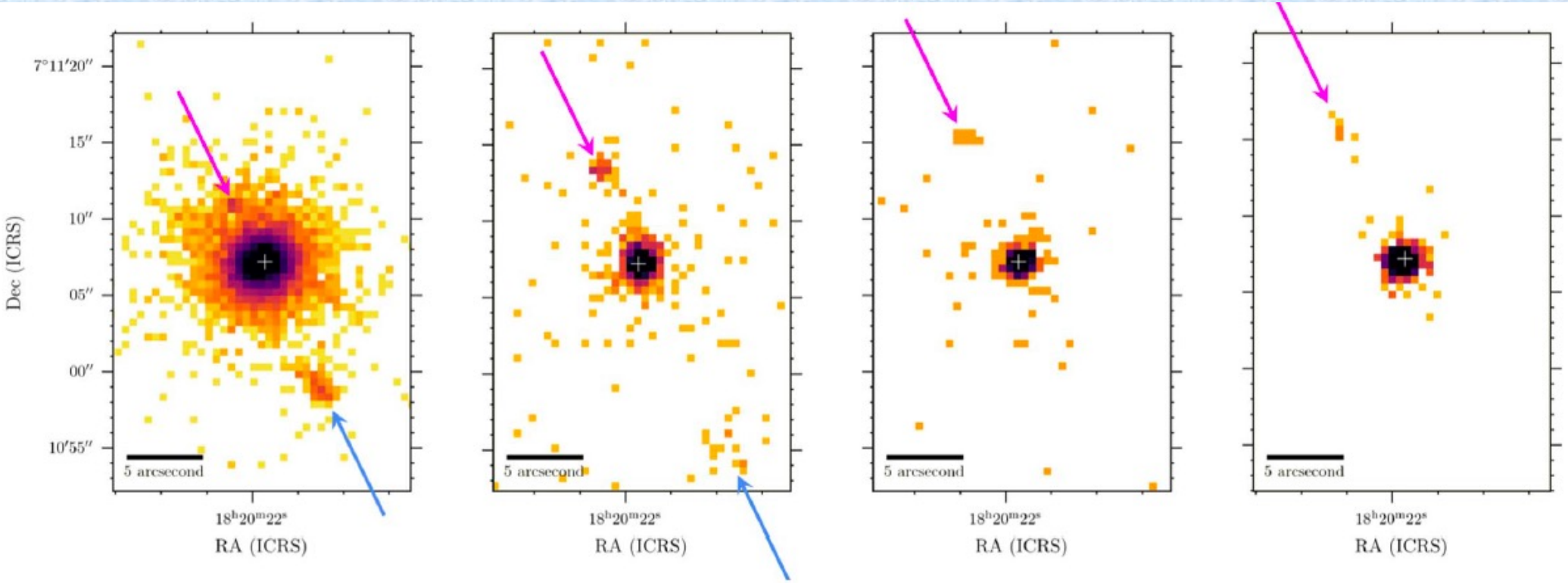

Figure 1. Images obtained from Chandra observations of MAXI J1820+070 in the 0.3–8 keV band. The observations are in chronological order: 2018 November, 2019 February, 2019 May, and 2019 June. The color scale is logarithmic and different for every image. The crosses indicate the VLBI position of MAXI J1820+070 (Atri et al. 2020). The arrows highlight the position of the north (pink) and south (blue) detected sources. The significances are, for the north and south jets, 46 and 43 (109 and 190 photons) in November and 16 and 4.2 (35 and 15 photons) in February; and for the north jet, 3.5 (6 photons) in May and 4.9 (12 photons) in June.

PA=25.1±1.4 deg (approaching jet at PA=205.1±1.4 deg)

Espinasse et al. (2020)

5. DIPol-2

MAXI J1820+070 in outburst

- In the rising hard state (HS) when the winds are present polarization degree (PD)=0.3-0.5%.
- Polarization angle (PA) during the HS coincides with the jet position angle. An additional component with a different PA likely contributes to the B-band.
- In the decaying HS, when the winds are absent also the intrinsic polarization is absent. Emission is dominated by (unpolarized) nonthermal component (jet or hot flow).
- In the soft state, optical emission is dominated by the irradiated disc and PA (-16 deg) and PD (0.2%) likely reflect that.

6. DIPol-UF

MAXI J1820+070 in quiescence

was observed with DIPol-UF @ NOT in July 2019, April 2020, July 2020, and July 2021

Date	B		V		R	
(MJD)	PD (%)	PA (deg)	PD (%)	PA (deg)	PD (%)	PA (deg)
			Outburst			
58195–58222	0.28 ± 0.01	9.2 ± 1.0	0.36 ± 0.01	22.9 ± 1.0	0.30 ± 0.01	29.0 ± 0.9
58223–58234	0.34 ± 0.02	8.8 ± 1.4	0.51 ± 0.02	23.4 ± 1.4	0.53 ± 0.02	23.9 ± 1.1
58312–58344	0.16 ± 0.01	-15.8 ± 1.6	0.15 ± 0.01	13.4 ± 2.3	0.02 ± 0.01	39.1 ± 11.0
58406–58428	0.06 ± 0.04	-3.0 ± 15.4	0.13 ± 0.06	2.8 ± 12.4	0.09 ± 0.04	44.8 ± 12.5
			Quiescence			
58686.93	3.86 ± 0.29	-23.8 ± 2.1	1.81 ± 0.24	-23.8 ± 3.8	0.70 ± 0.14	-24.1 ± 5.7
58688.01	2.35 ± 0.38	-25.9 ± 4.7	1.09 ± 0.25	8.0 ± 6.5	1.70 ± 0.10	-42.4 ± 1.7
58961.15	1.47 ± 0.28	-26.8 ± 5.4	0.52 ± 0.24	-4.2 ± 13.3	0.63 ± 0.19	8.5 ± 8.7
58964.16	4.31 ± 0.28	-18.5 ± 1.8	3.10 ± 0.29	-17.5 ± 2.7	1.05 ± 0.18	-2.0 ± 4.8
58965.11	2.81 ± 0.24	-23.5 ± 2.5	2.12 ± 0.21	-35.1 ± 2.9	0.84 ± 0.18	-26.3 ± 6.2
58967.12	4.53 ± 0.28	-24.1 ± 1.8	2.09 ± 0.39	-11.0 ± 5.3	1.09 ± 0.31	-27.0 ± 8.3
59050.94	4.58 ± 0.34	-15.3 ± 2.1	3.57 ± 0.31	-16.5 ± 2.5	1.54 ± 0.18	-14.5 ± 3.4
59050.98	5.03 ± 0.30	-11.0 ± 1.7	3.38 ± 0.34	-11.7 ± 2.9	1.62 ± 0.16	0.3 ± 2.9
59051.05	3.35 ± 0.26	-23.5 ± 2.2	2.04 ± 0.23	-17.1 ± 3.2	1.08 ± 0.18	-12.1 ± 4.9
59051.10	3.14 ± 0.30	-10.7 ± 2.7	1.95 ± 0.29	-4.8 ± 4.3	0.95 ± 0.16	5.6 ± 4.9
59051.92	4.08 ± 0.27	-18.1 ± 1.9	3.40 ± 0.25	-12.9 ± 2.1	1.39 ± 0.15	-18.0 ± 3.1
59051.97	4.67 ± 0.30	-16.5 ± 1.8	3.27 ± 0.30	-17.5 ± 2.6	1.96 ± 0.15	-17.9 ± 2.2
59052.03	4.83 ± 0.31	-16.7 ± 1.9	3.37 ± 0.24	-10.3 ± 2.1	1.68 ± 0.15	-20.0 ± 2.6
59052.09	3.78 ± 0.23	-21.5 ± 1.7	2.47 ± 0.22	-28.0 ± 2.5	1.06 ± 0.16	-12.4 ± 4.3
59052.92	4.14 ± 0.23	-24.2 ± 1.6	2.46 ± 0.23	-16.6 ± 2.7	1.21 ± 0.14	-18.4 ± 3.3
59052.98	3.30 ± 0.28	-20.5 ± 2.4	2.18 ± 0.23	-23.6 ± 3.0	1.18 ± 0.17	-14.0 ± 4.0
59053.92	4.02 ± 0.25	-12.8 ± 1.8	2.22 ± 0.26	-3.5 ± 3.4	1.24 ± 0.15	0.2 ± 3.4
59053.97	4.30 ± 0.27	-16.5 ± 1.8	3.18 ± 0.24	-10.4 ± 2.1	1.51 ± 0.15	-13.1 ± 2.9
59400.99	1.62 ± 0.12	-30.5 ± 2.0	0.77 ± 0.10	-17.1 ± 3.9	0.41 ± 0.07	6.4 ± 5.1
59401.94	2.86 ± 0.21	-25.4 ± 2.1	2.04 ± 0.20	-29.9 ± 2.8	0.36 ± 0.14	-6.1 ± 10.7
59051–59054	4.00 ± 0.19	-17.5 ± 1.3	2.65 ± 0.19	-14.7 ± 1.9	1.32 ± 0.08	-12.8 ± 2.3
58686–59402	3.18 ± 0.22	-19.7 ± 1.2	1.89 ± 0.19	-16.8 ± 1.9	0.94 ± 0.11	-18.6 ± 3.3
			Interstellar polarization			
58195–59054	0.81 ± 0.03	64.0 ± 1.1	0.71 ± 0.03	68.4 ± 1.2	0.60 ± 0.02	64.4 ± 0.8

6. DIPol-UF

MAXI J1820+070 in quiescence

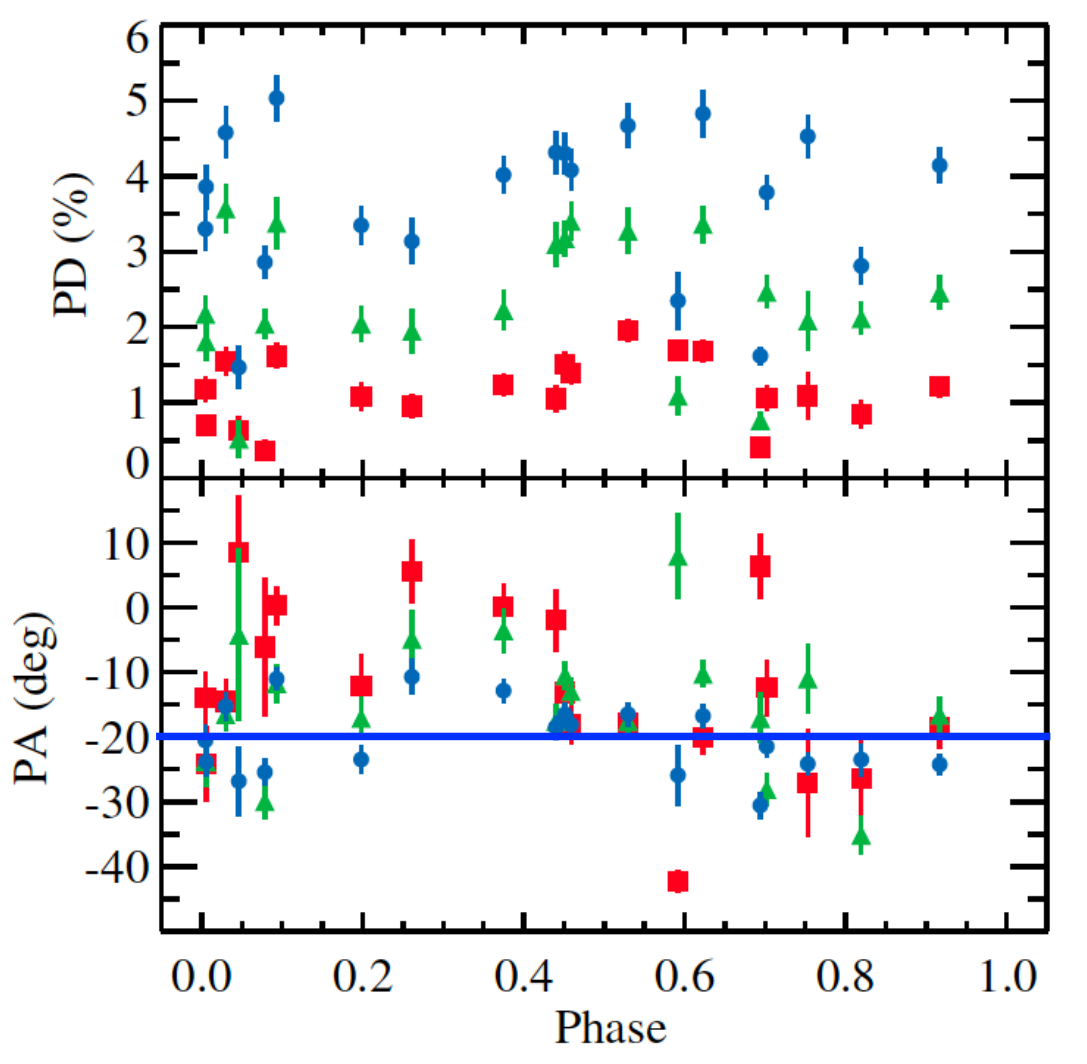

MAXI J1820+070 was observed with DIPol-UF @ NOT in July 2019, April 2020, July 2020, and July 2021

1. PD is 1-5%, very blue
2. PD is variable, no obvious orbital dependence
3. PA is very different from that observed in the hard state during outburst.
4. $\langle PA_B \rangle = -19.7^o \pm 1.2^o$

Poutanen et al. (subm.)

MAXI J1820+070 in quiescence

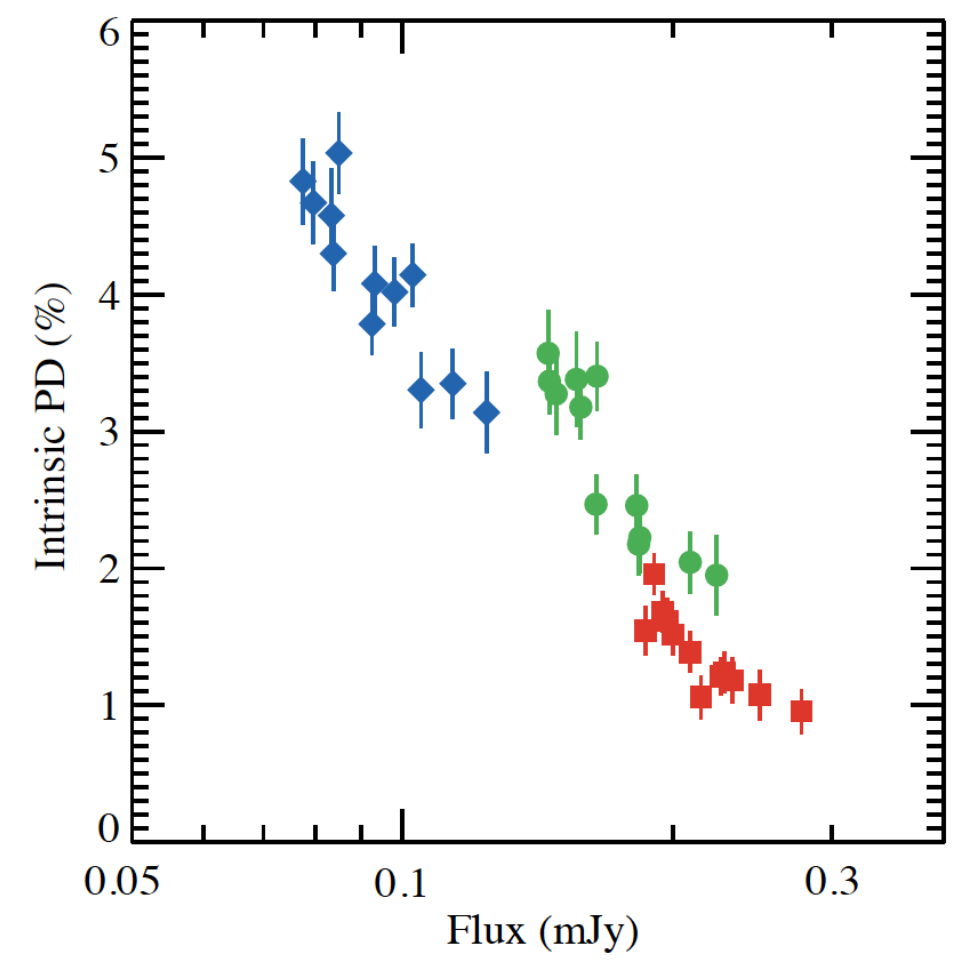

Observations in July 2020: flux is anticorrelated with PD.

Likely results from the presence of a more variable red unpolarized component.

BH spin – orbital spin misalignment β

Jet inclination $i_{bh} = 63^o \pm 3^o$
(Atri et al. 2020)

Disc inclination $i_{orb} = 73^o \pm 6^o, < 81^o$
(Torres et al. 2020)

$PA_{jet} = \theta_{bh} = 25.1^o \pm 1.4^o$
(Espinasse et al. 2020)

Assume
$\theta_{orb} = PA = -19.7^o \pm 1.2^o$

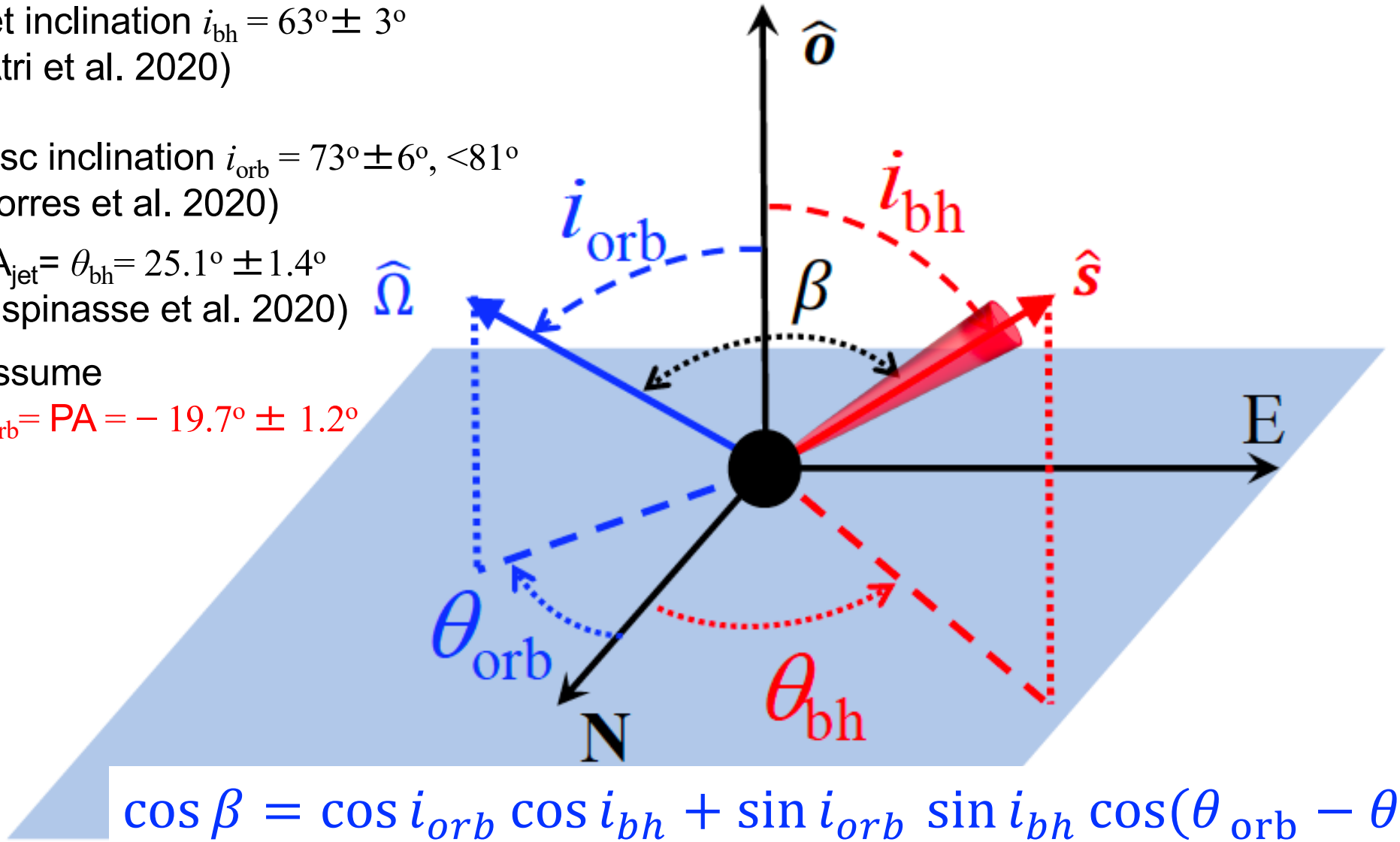

$$\cos\beta = \cos i_{orb} \cos i_{bh} + \sin i_{orb} \sin i_{bh} \cos(\theta_{orb} - \theta_{bh})$$

BH spin azimuthal angle (in the orbital plane)

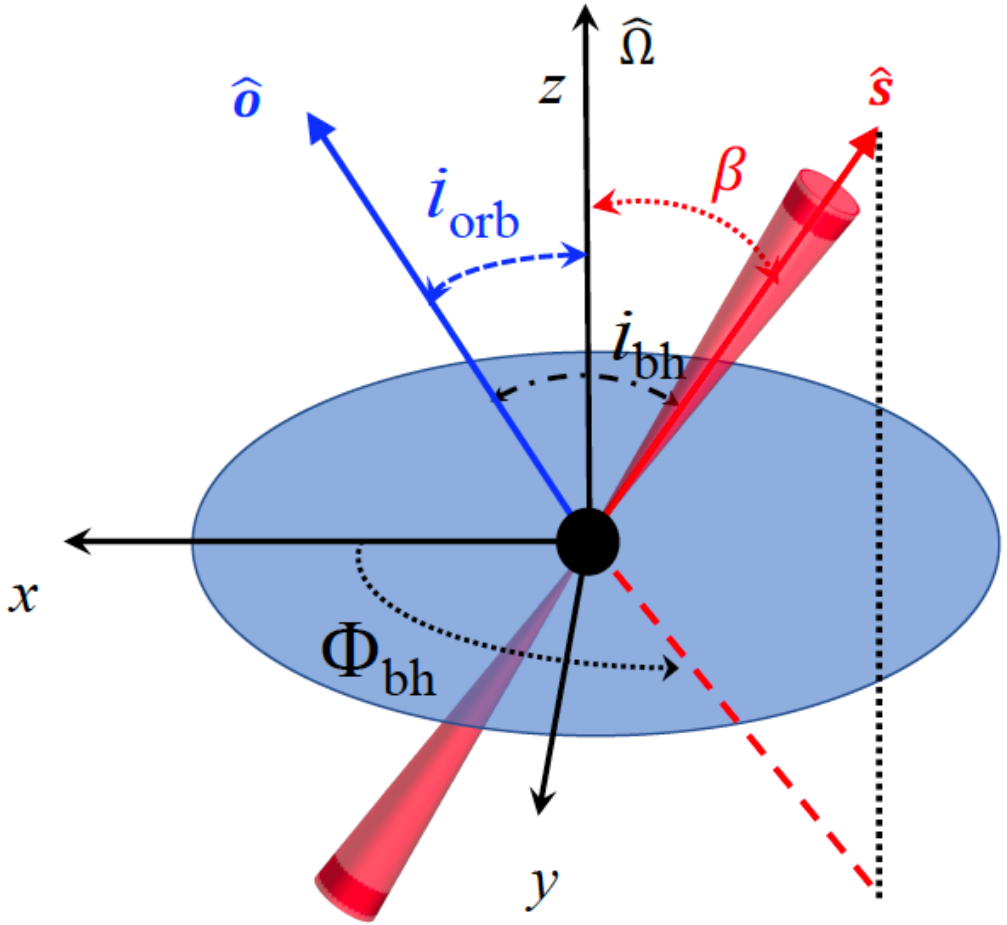

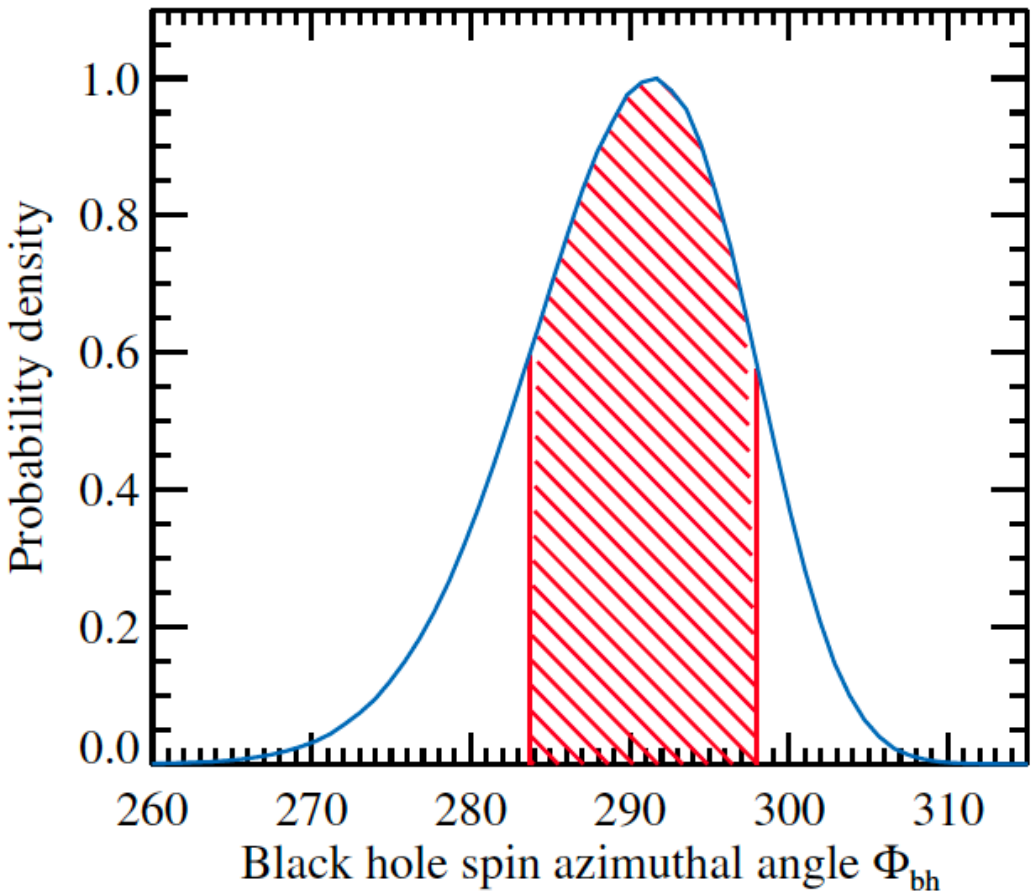

$$\cos\Phi_{\rm bh} = \frac{\sin i_{\rm orb}\cos i_{\rm bh} - \cos i_{\rm orb}\sin i_{\rm bh}\cos\Delta}{\sin\beta}$$

$$\sin\Phi_{\rm bh} = -\frac{\sin i_{\rm bh}\sin\Delta}{\sin\beta}.$$

$$\Delta = \theta_{\rm orb} - \theta_{\rm bh}$$

MAXI J1820+070 in quiescence

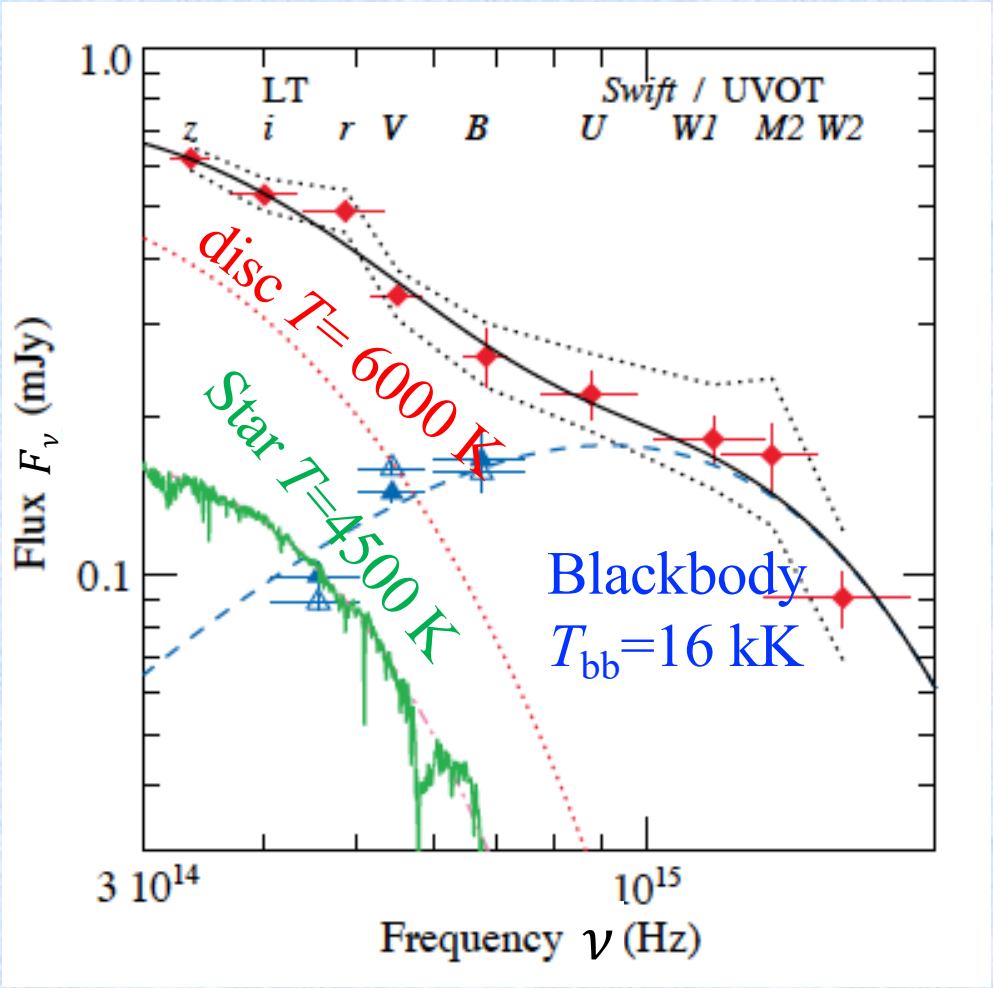

Poutanen et al. (subm.)

The polarized flux is consistent with the constant PD of ~6% of the UV "blackbody" component

$$PF_E = F_E \times \mathrm{PD}_E$$

$$PF_E = P \times B_E$$

Parameter	Value	Units
T_{in}	6190±750	K
R_{in}	$(6.4 \pm 1.5) \times 10^{10}$	cm
T_{bb}	16300±2000	K
R_{bb}	$(7.6 \pm 1.9) \times 10^{9}$	cm
T_*	4500	K
R_*	5×10^{10}	cm
P_{UV}	0.066 ± 0.017	

Nature of polarized UV excess

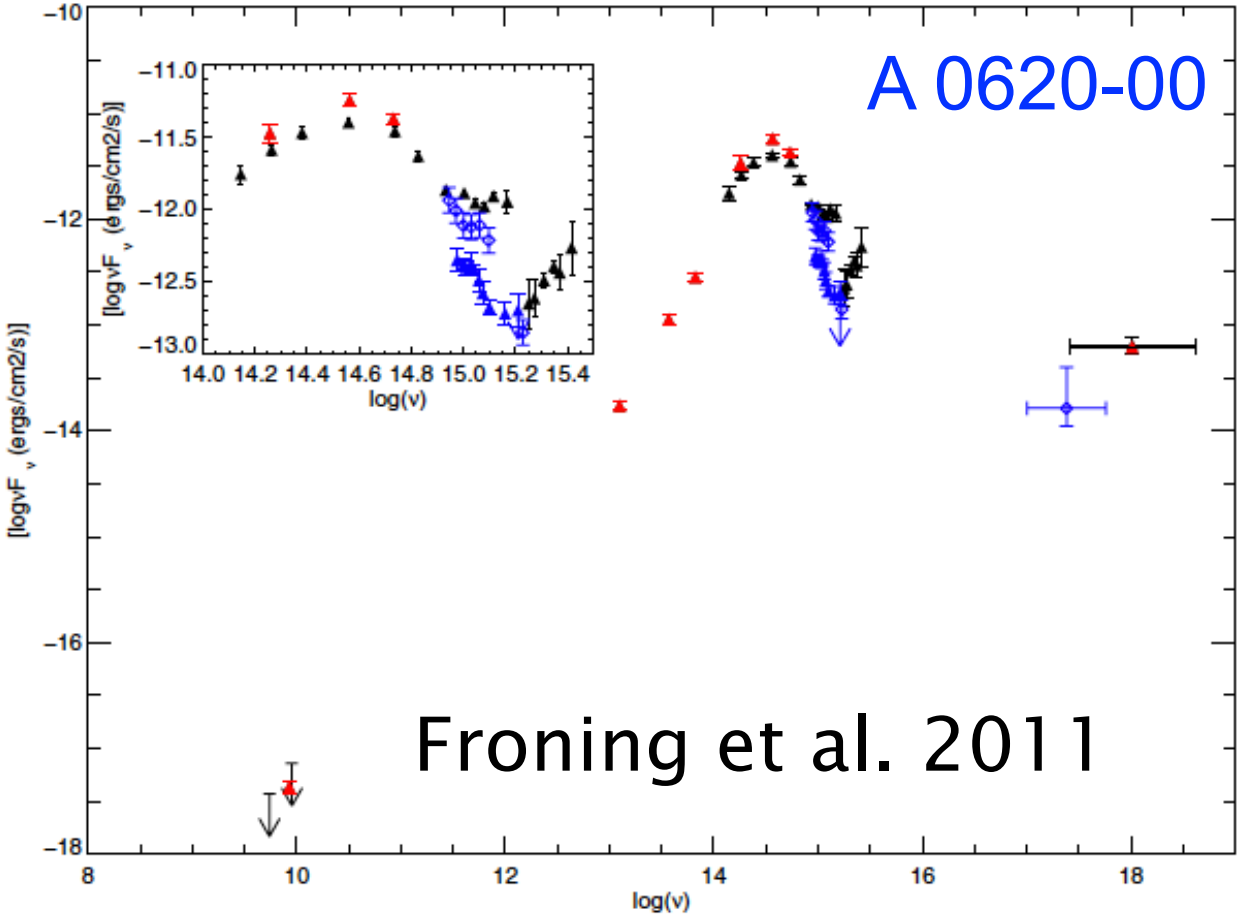

Figure 5. Broadband spectral energy distribution for A0620-00. The full SED from radio to X-rays is shown in the main window while the inset gives an expanded view of the NIR/optical/UV range. The solid black triangles are from this work. The red points show the data from Gallo et al. (2007, 2006) while the blue points are taken from Narayan et al. (1996) (FOS data; open triangles) and McClintock & Remillard (2000) (STIS data, closed triangles). Only the data >3500 Å are shown from the latter two sources because their points at longer wavelengths have had the donor star contribution removed. All the data have been dereddened using the extinction relation of Cardelli et al. (1989) assuming $E(B-V) = 0.35$. (Gallo et al. originally used a reddening of 0.39 but we have shifted their points to the common value.)

Nature of polarized UV excess

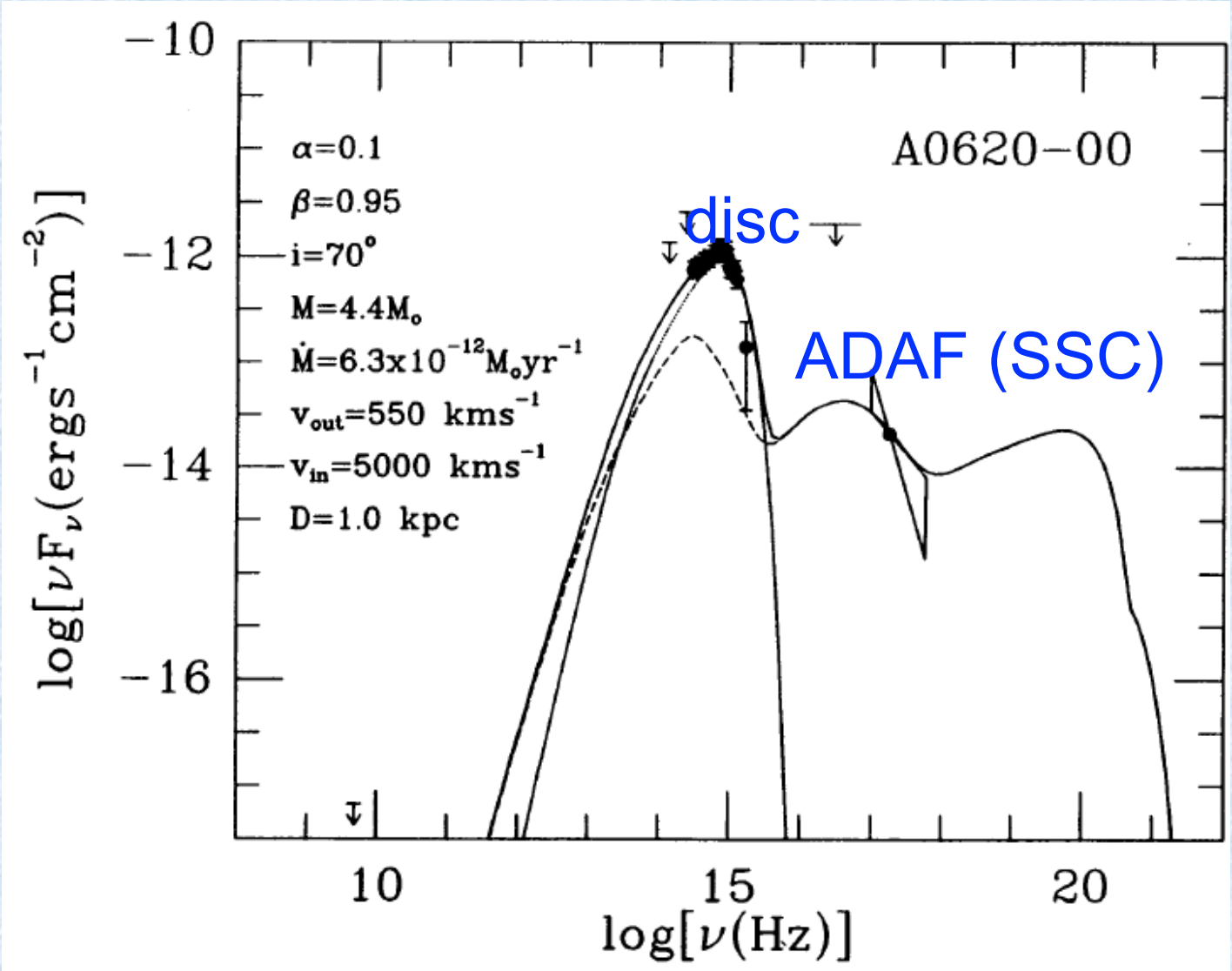

Fig. 1 from Narayan et al. 1996, ApJ, 457, 821

Nature of polarized UV excess

- ADAF can produce UV excess, but
- SSC model for (nearly spherical) ADAF with tangled magnetic field cannot produce high PD.
- However, disc Comptonization in ADAF can.
- Photons (Thomson) scattered in a plane attain PD up to 33% (Sunyaev & Titarchuk 1985):

$$P = \frac{1-\mu^2}{3-\mu^2}, \quad \mu = \cos i_{orb}$$

- Polarization vector is perpendicular to the disc plane.
- Scattering by hot electrons reduces PD (Poutanen 1994).
- Scattering in a thick hot flow also reduces PD.

Nature of polarized UV excess

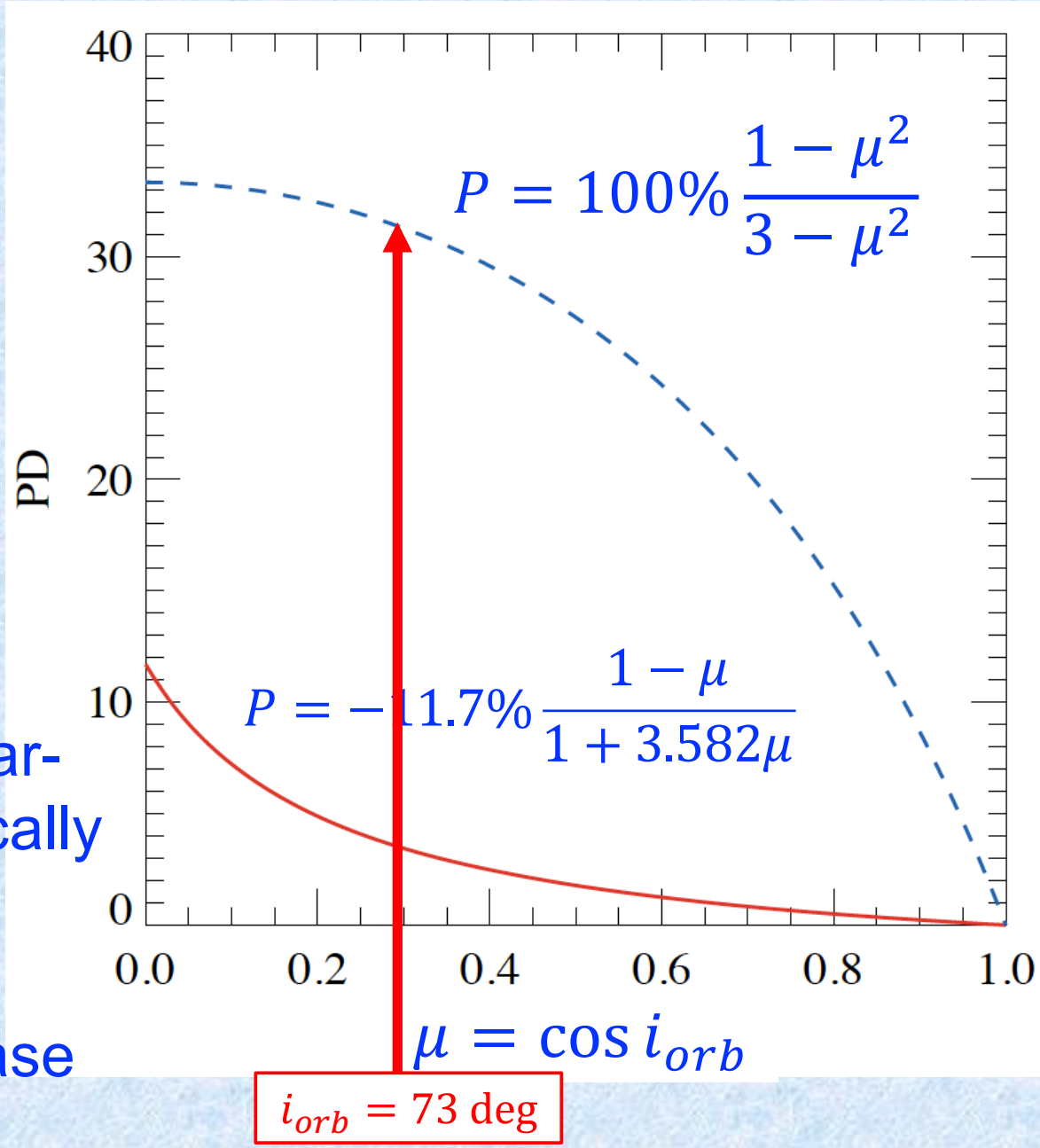

Chandrasekhar-Sobolev (optically thick electron scattering dominated) case

Modelling polarized UV excess

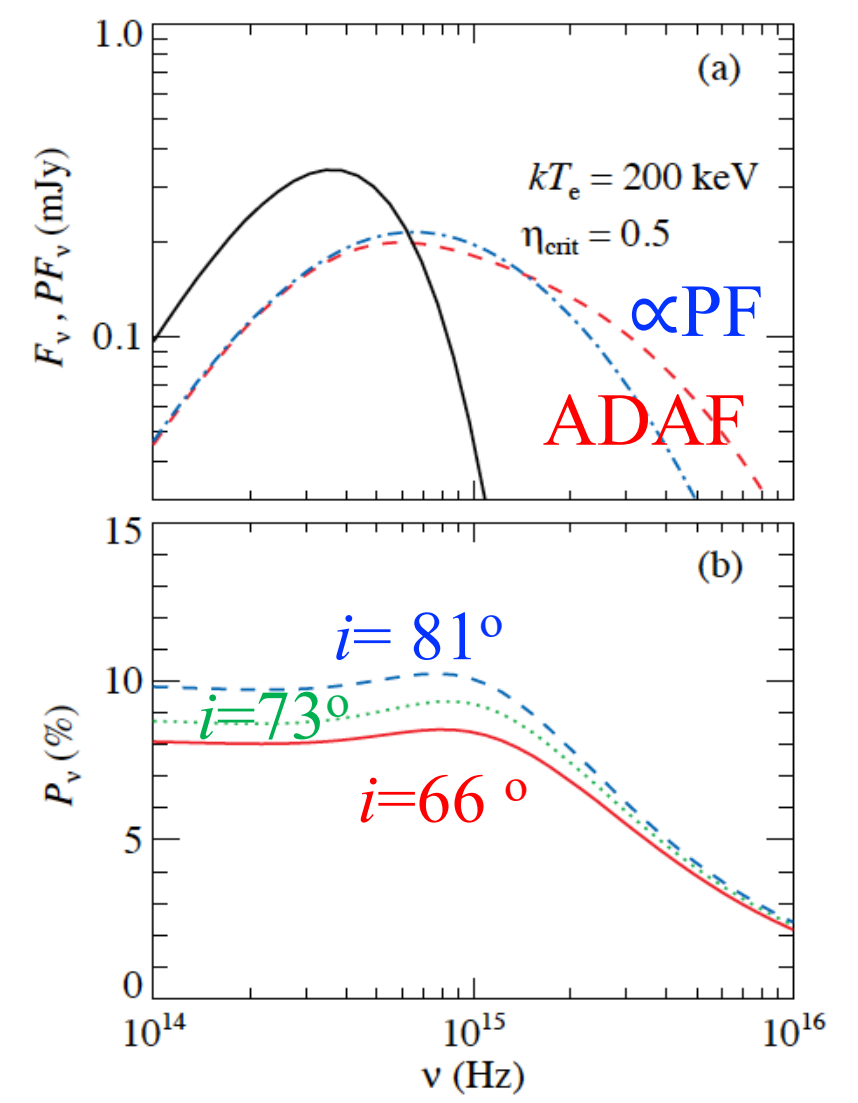

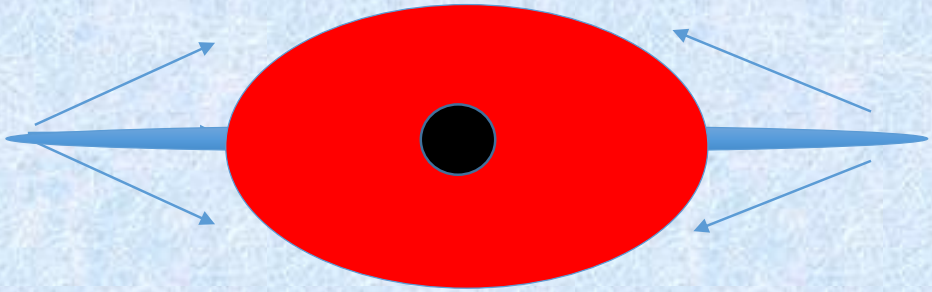

- Higher electron temperature would reduce PD.
- Lower electron temperature would reduce disc photons energy shift.

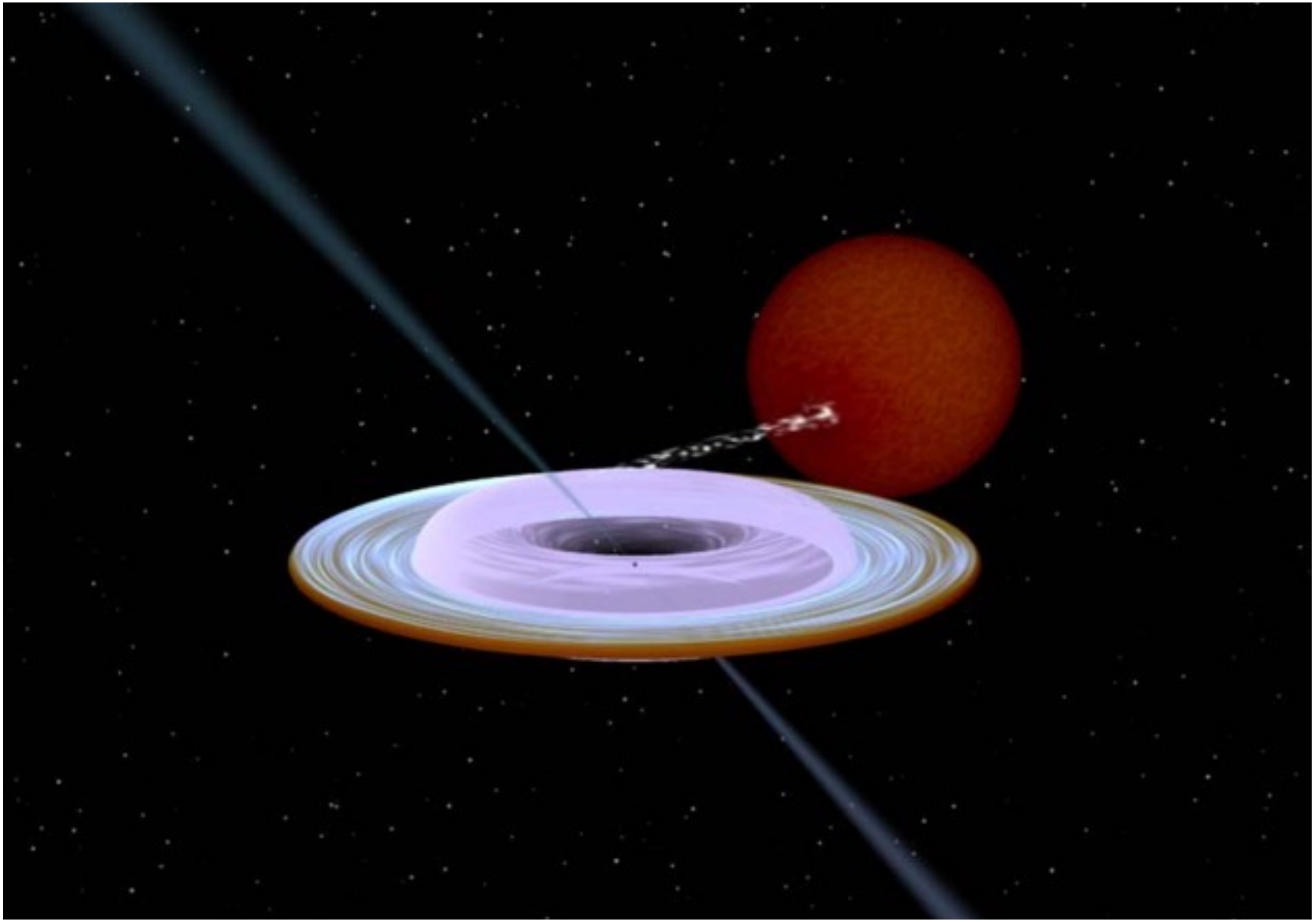

IXPE
Imaging
X-Ray
Polarimetry
Explorer

IMAGING X-RAY POLARIMETER EXPLORER

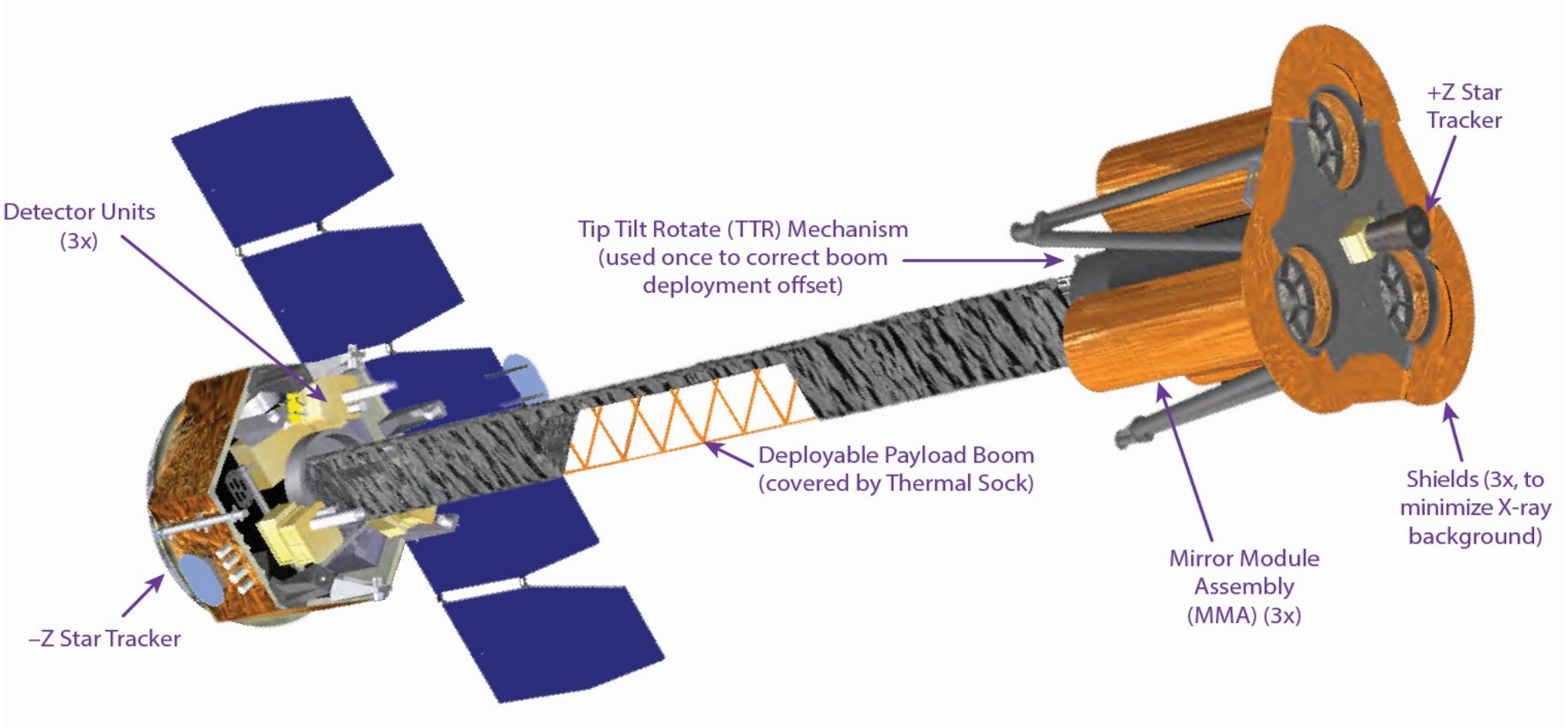

First dedicated space X-ray polarimeter to be launched on Dec 9, 2021!

IXPE
Imaging X-Ray Polarimetry Explorer

MEASURE BLACK-HOLE SPIN FROM POLARIZATION ROTATION IN TWISTED SPACE-TIME

- **Accreting black holes (GRS 1915+105, Cyg X-1) in soft state**
  - Scattering polarizes the thermal disk emission
  - Polarization rotation is greatest for emission from inner disk (Connors et al. 1980). Inner disk is hotter, producing higher energy X-rays
  - Priors on disk orientation constrain the black hole spin
    - a = 0.50±0.04; 0.900±0.008; 0.99800±0.00003 (200-ks observation)

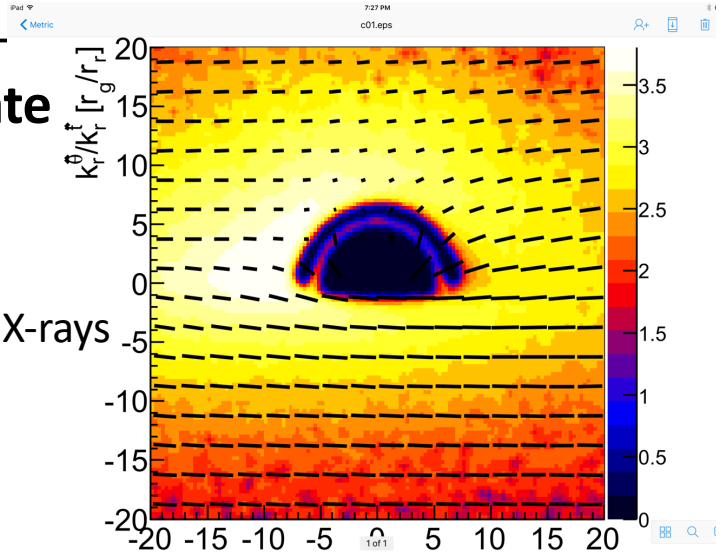

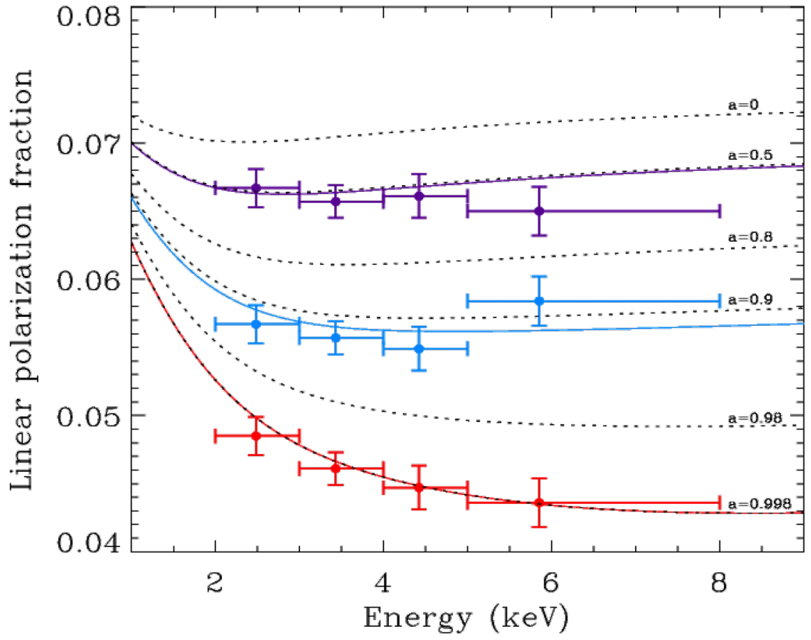

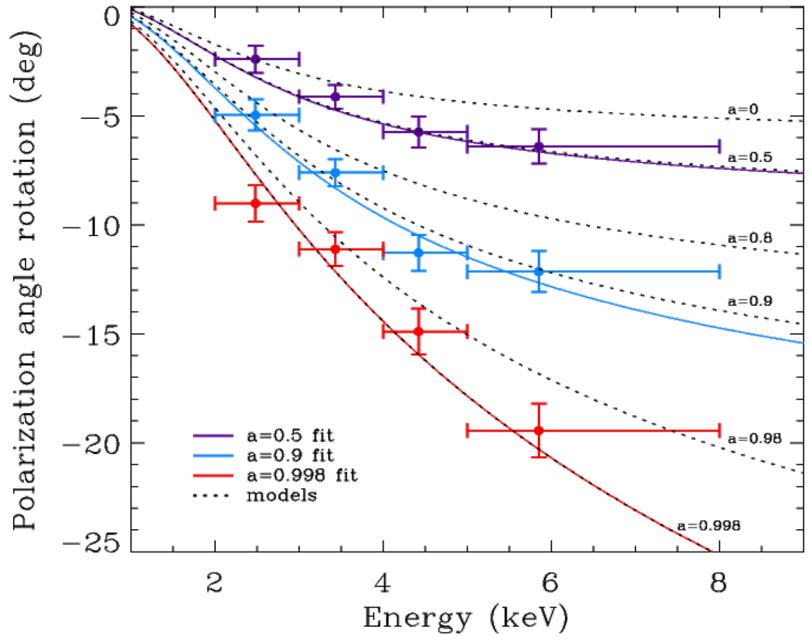

IXPE
Imaging
X-Ray
Polarimetry
Explorer

TEST THEORIES OF QPO PRODUCTION

- **Accreting black holes (Cyg X-1, transients) in hard state**

Polarization pattern will vary with the QPO phase (Ingram, Maccarone, JP, Krawczynski 2015).

Theory for Comptonization of polarized radiation developed in Poutanen & Svensson (1996).

Analytical theory for computing Stokes vector from accretion disk in Loktev, Veledina, JP (2021).

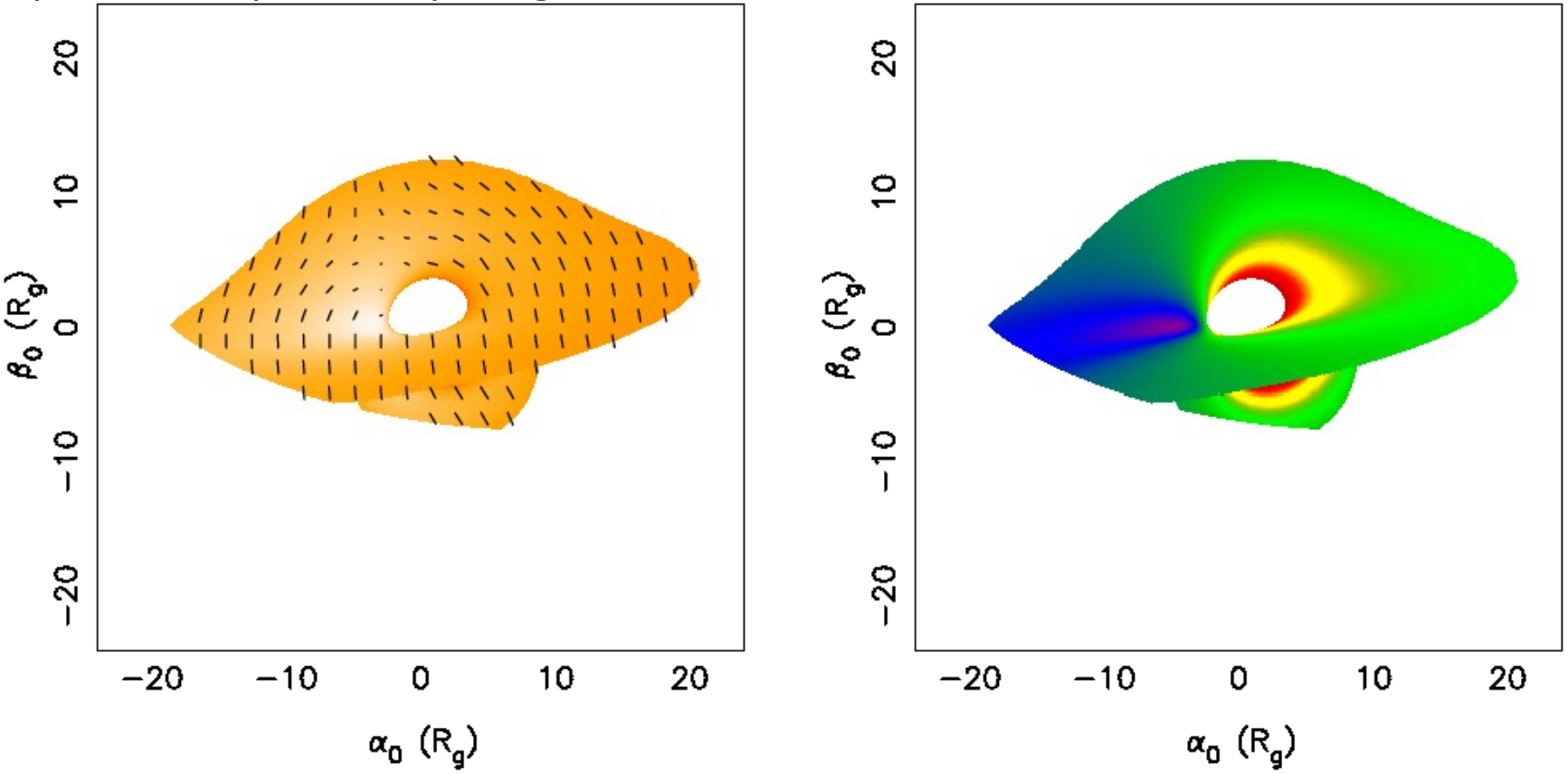

IXPE
Imaging
X-Ray
Polarimetry
Explorer

TEST THEORIES OF QPO PRODUCTION

- **Accreting black holes (Cyg X-1, transients) in hard state**

  Polarization pattern will vary with the QPO phase (Ingram, Maccarone, JP, Krawczynski 2015)

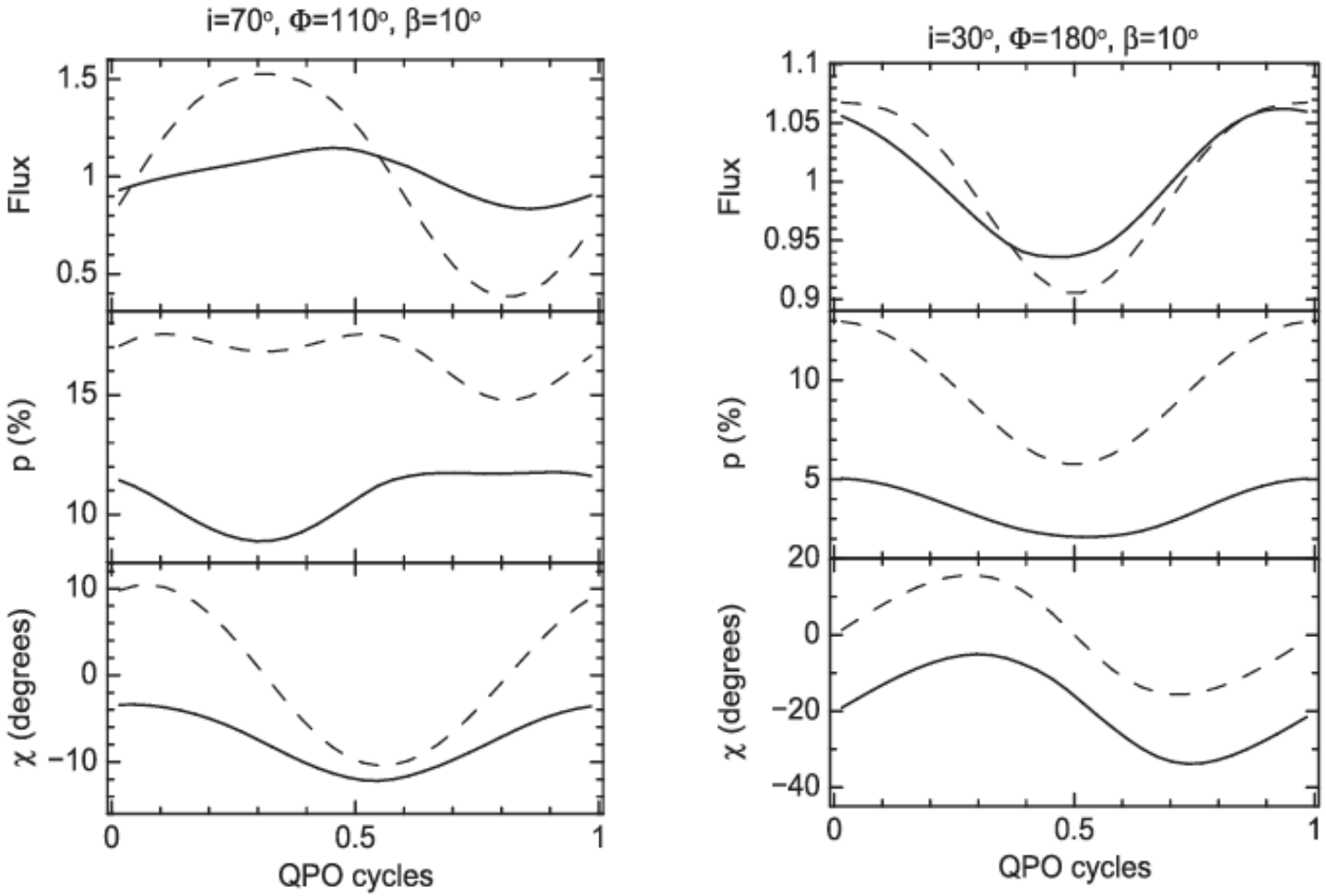

Conclusions

- High-precision optical polarimeters DIPol-2 and DIPol-UF have been used to detect intrinsic polarization in two black hole transients V404 Cyg and MAXI J1820+070.
- ISM polarization was accurately subtracted using field stars located at similar distances.
- V404 Cyg shows intrinsic PD=0.5-1% rising towards blue. Likely is produced in an optically thick envelope (wind). PA varies between -30 and 0 deg, similarly to the jet position angle.
- MAXI J1820+070 in the outbursts shows PD=0 in the decaying hard state (when there are no winds). PD=0.3-0.5% in the rising hard state (when winds are detected) with PA=25 deg, parallel to the jet. Likely produced by the wind. The soft state PD<0.2%, with PA_B=-16 deg, likely produced by irradiated disc.
- MAXI J1820+070 in its quiescent state shows high (1-5%) PD rising towards blue.
- Polarized flux is very hard, consistent with the extension to the UV excess. Polarized UV excess may be related to scattering of the disc radiation by hot (200 keV) medium in the inner hot flow (ADAF).
- PA differs from the jet position angle by ~45 deg. This translates to at least 40 deg misalignment between the jet (BH spin) and the disc (orbital spin) axis.
- Large misalignment has profound implications for the models of black hole formation, models of X-ray and optical QPOs (Lense-Thirring precession), reliability of BH spin measurements from iron line, BH mass measurements, etc.
- Future X-ray polarimetric observations with IXPE can be used to test disc orientation and QPO production mechanism.